Localization of the *Agrobacterium tumefaciens* Type IV Secretion System and its role in host cell attachment

by

Julieta Aguilar

A dissertation submitted in partial satisfaction of the requirements for the degree of

Doctor of Philosophy
in

Microbiology
in the

Graduate Division
of the

UNIVERSITY OF CALIFORNIA, BERKELEY

Committee in charge:

Patricia Zambryski, Chair
Arash Komeili
Mary Wildermuth

Spring 2011

Abstract

Localization of the *Agrobacterium tumefaciens* Type IV Secretion System and its role in host cell attachment

by
Julieta Aguilar
Doctor of Philosophy in Microbiology
University of California, Berkeley
Professor Patricia C. Zambryski, Chair

The interaction between *Agrobacterium tumefaciens* and its plant host is a classic model system for investigating host pathogen interactions. Significant progress has been made in various aspects of *A. tumefaciens* mediated genetic transformation of plants, which leads to the formation of crown gall tumors. It is known that wounded plant cells release phenolic compounds induces the expression of the transformation products, the T-strand and virulence (Vir) proteins, which are encoded on the tumor-inducing plasmid (pTi). The Vir proteins assemble a translocation channel called the virulence-induced type IV secretion system (*vir*-T4SS). The T-strand is a single stranded segment of DNA that gets integrated into the host plant cell and the expression of the genes on the T-strand causes crown gall tumors.

The *vir*-T4SS is composed of 11 VirB proteins and VirD4, and all 12 components are essential for maximal DNA and protein transport. These components can be divided into 3 major groups. The first group consists of the T-pilus and its associated components (VirB1, VirB2, VirB3, and VirB5). VirB1 has homology to lytic transglycolases and is likely to cleave the peptidoglycan to facilitate assembly of the *vir*-T4SS. VirB2 is the major component of T-pilus, and VirB5 is localized at the T-pilus tip. VirB1 and VirB3 are required for T-pilus assembly. The second group consists of the core transport complex that spans the inner and outer membranes and periplasm (VirB6-VirB10). The third group consists of the energetic components (VirB4, VirB11, and VirD4). These components have ATPase homology and ATP-binding motifs, and may energize the assembly and transfer of DNA and proteins through the *vir*-T4SS. VirD4 is also the coupling protein that brings DNA and *vir*-T4SS substrate proteins to the *vir*-T4SS. The *vir*-T4SS transports the T-strand, and at least 4 Vir protein substrates (VirD2, VirE2, VirE3, and VirF) into the host cell. It is estimated that 50 T-strands and thousands of VirE2, VirE3, and VirF proteins are all transported through the *vir*-T4SS. However, it still remains unclear how many *vir*-T4SS are localized on the bacterial cell and how the *vir*-T4SS interacts with the host cell to transport the T-strand and the *vir*-T4SS protein substrates.

It was proposed that most Vir proteins were localized at the pole of *A. tumefaciens* and that *A. tumefaciens* attached to host cells via its poles. However, early studies from the Zambryski lab suggested that at least one component of the T4SS, VirB8, localized around the bacterial perimeter in transverse-section and in multiple sites in longitudinal section of *vir*-induced cells. Other studies suggested that not all T4SS components localize to the same position perhaps suggesting subassemblies. Therefore, to clear these inconsistencies and to identify how many *vir*-T4SS are localized on the bacterial cell and to better understand how the *vir*-T4SS interact with the host cell to transport the T-strand and the *vir*-T4SS protein substrates, I analyzed the localization of the *vir*-T4SS components and substrates in the presence and absence of its host.

I cloned the structural components of the *vir*-T4SS and the *vir*-T4SS substrates as GFP fusion vectors for induced expression in the two most common lab strains of *A. tumefaciens*. After induction, GFP fusions were imaged by high-resolution deconvolution microscopy. Tumorigenesis assays were used to test the functionality of fusion proteins. I found that those that carried a cytoplasmically localized GFP retained their functions, while those with predicted periplasmic GFP and GFP fusions to VirB10 had a dominant-negative effect on tumor formation. Thus, suggesting the addition of GFP to these proteins may interfere with the correct assembly and proper function of the *vir*-T4SS. Three-dimensional reconstruction of the deconvolved images revealed that most of the proteins were found in multiple foci around the cell periphery. I confirmed these findings by examining endogenous protein patterns by immunofluorescence microscopy. Extensive quantitative analyses also verified that the Vir proteins of the *vir*-T4SS are localized to multiple foci around the periphery of the Agrobacterial cell. In support, I found multiple T-pili on bacterial cells. Interestingly, the localization of the *vir*-T4SS components resembled a helical pattern. Other proteins that form helical patterns are bacterial cytoskeletal components, such as MinD. In fact, VirB8 and MinD colocalize suggesting that cytoskeletal components may provide an existing scaffold for *vir*-T4SS assembly. Furthermore, I found that Agrobacteria attaches predominantly laterally to host cells and few cells attach at their poles. Also, the localization of the *vir*-T4SS does not change upon contact to host cells suggesting that perhaps multiple *vir*-T4SS are utilized.

In summary, my results revealed that the *vir*-T4SS is localized around the perimeter of the cell resembling a helical pattern, and that *A. tumefaciens* attached to host cells predominantly along their sides. My work challenges the existing paradigm of polar localization and orientation of attachment and has led to a novel model with multiple *vir*-T4SS around the bacteria. This would maximize the possibility for effective attachment along the bacterial length, which may allow efficient transfer of numerous amounts of T-strands and thousands of protein substrates into the host cell.

para mi abue

(December 12,1925-April 21, 2011)

Guadalupe Martinez de Aguilar

Thank you for all your love and support throughout the years.
“Te quiero mucho abue”

Table of Contents

Abstract 1

Table of Contents ii

List of Figures iii

List of Tables iv

List of Movies v

Chapter 1: Introduction 1

Chapter 2: *Agrobacterium* type IV secretion system and its substrates form helical arrays around the circumference of *virulence*-induced cells 10
- Abstract 11
- Introduction 11
- Results 12
- Discussion 22
- Materials and Methods 26
- Acknowledgements 27

Chapter 3: Membrane and core periplasmic components of the virulence induced type IV secretion system of *Agrobacterium tumefaciens* localize to multiple sites around the bacterial perimeter 28
- Abstract 29
- Introduction 29
- Results 31
- Discussion 39
- Materials and Methods 42
- Acknowledgements 43

References 44

List of Figures

Figure 1. Overview of *Agrobacterium tumefaciens* mediated transformation of a plant cell....8

Figure 2. The virulence induced type IV secretion system of *Agrobacterium tumefaciens* 9

Figure 3. GFP-VirB8 localizes to a helical array of foci in *vir*-induced *Agrobacterium* 14

Figure 4. GFP-VirB8 colocalizes with RFP-MinD 15

Figure 5. T4SS substrates VirD2, VirF, and VirE2 localize to a helical array of foci in *vir*-induced *Agrobacterium* 18

Figure 6. Expression levels of GFP fusion proteins....19

Figure 7. Localization patterns of GFP fusions to T4SS components, VirB6, VirB7, VirB9, VirB10, VirB11, and VirD4....20

Figure 8. Time course of T4SS and T4SS substrate localization 21

Figure 9. Detection of T-pili in *vir*-induced *Agrobacterium* and during attachment to the plant cell surface....23

Figure 10. Model for T4SS localization and function during binding to plant cells....24

Figure 11. Immunofluorescent detection of VirB proteins in *vir*-induced *A. tumefaciens* nopaline strain (C58)....34

Figure 12. Localization of octopine VirB8 in *vir*-induced *A. tumefaciens* octopine strain (A348)....35

Figure 13. Detection of VirB proteins in *A. tumefaciens* A348....36

Figure 14. *A. tumefaciens* attachment to host cell(s)....38

Figure 15. Model for the localization of *vir*-T4SS and lateral attachment of *A. tumefaciens* to a plant cell....40

List of Tables

Table 1. Cellular localization of VirB proteins 33

Table 2. Labeling specificity of VirB antibodies 33

List of Movies

Movie 1. 3D deconvolved movie of free GFP in wild type C58 *Agrobacterium* ..... CD

Movie 2. 3D deconvolved movie of GFP-VirB8 in wild type C58 *Agrobacterium* ..... CD

Movie 3. 3D deconvolved movie of GFP-VirB8 in ΔVirB8 *Agrobacterium* ..... CD

Movie 4. 3D deconvolved movie of native VirB8 in wild type C58 *Agrobacterium* detected by immuno-fluorescence ..... CD

Chapter 1

Introduction

Bacteria have evolved several systems to sense and respond to their environments or interact with other cells. Protein secretion systems in bacteria play a crucial role in modulating these interactions by secreting proteins to the extracellular milieu or translocating effectors or toxins into host cells (Tseng et al., 2009). There are seven general classes of secretion systems (Type I-VII). The Type I secretion system (T1SS) is composed of the ATP-binding cassette (ABC) transporter, outer membrane factors (OMFs), and the membrane fusion proteins. The type II secretion system (T2SS) also known as the sec-dependent pathway or the general secretory pathway is composed of 23-29 proteins that span the inner and outer membrane. The type III secretion system (T3SS), also known as the injectisome, has homology to the flagellum and is composed of up to 25 proteins. The type IV secretion system (T4SS) is unique from the other secretion systems since is able to transport DNA and proteins. In the archetypal T4SS of *A. tumefaciens* is composed of 12 proteins. The type V secretion system (T5SS) are also known as the autotransporters, since the C-terminal domain can form a beta barrel forming the translocation pore where the N-terminal domain could pass through. The type VI secretion system (T6SS) is a recently characterized secretion system analogous to the T3SS and T4SS. The type VII secretion system (T7SS) is a newly discovered secretion system found in Gram-positive bacteria and its structure remains unknown. In Gram-negative bacteria, T1SS, T3SS, T4SS, and T6SS export molecules to the extracellular space by causing transport across the inner membrane, periplasm, and outer membrane in a single step. In T2SS, molecules reach the extracellular space in two-steps. First molecules are translocated to the periplasm through the general secretory pathway and then pass through the translocation pore in the outer membrane. In Gram-positive bacteria molecules are transported through similar secretion systems plus the T7SS, which is specific to Gram-positive bacteria. Bacterial secretion systems are particularly important in pathogenesis where secreted molecules or transported molecules directly affect eukaryotic host cells.

Type IV Secretion System. One of the best-studied secretion systems that is used by both Gram-negative and Gram-positive bacteria and that is critical to pathogenesis is the T4SS. Type IV secretion systems allows the exchange of DNA between bacteria, the transport of DNA into plant cells, and the transport of effector proteins into eukaryotic cells. The T4SS is ancestrally related to bacterial conjugation machinery that transports DNA across the cell envelope to recipient bacterial cells (Christie, 2001). T4SS that are dedicated to conjugal DNA transfer of plasmids between bacteria are the F (IncF), RP4 (IncP), R388 (incW), pKM101 (IncN) plasmids. T4SS involved in pathogenesis transport effectors into host cells. For example, *Helicobacter pylori* uses its T4SS to transfer a 145kDa protein, CagA, to mammalian hosts to cause peptic ulcers. Other pathogens that cause disease by delivering effector proteins are *Legionella pneumophila,* which causes Legionnaires' disease, *Bordetella pertussis,* which causes whooping cough, and *Ricksettsai prowazekii*, which causes typhus fever (Zhu et al., 2011, O'Callaghan et al., 1999, Walker and Yu, 2005, Shrivastava and Miller, 2009). The virulence induced (*vir-)* T4SS of *A. tumefaciens* transports both DNA and

virulence (Vir) proteins across bacterial cell envelope and then through plant cell wall and membrane into the plant cytoplasm. The *vir*-T4SS of *A. tumefaciens* serves as a prototype for other T4SS because it is the best studied and their components are highly conserved.

Agrobacterium tumefaciens. *A. tumefaciens* is a Gram-negative, rod shape, motile bacterium, living in the rhizosphere. In agriculture, *A. tumefaciens* is a serious pathogen of walnuts, grape vines, stone fruits, and sugar beets. In the laboratory, *A. tumefaciens* has been established as an important model system and has provided fundamental insights into various biological processes such as: 1) chemical and physical communication between microbes and plants, 2) DNA and protein transport across kingdoms, 3) vectors for plant transformation, 4) quorum sensing, 5) spreading of antibiotic resistance genes and other virulence proteins among bacteria, and 6) identification of the requirements for nuclear uptake of proteins following transport across kingdoms. Additionally, it has been useful in the genetic engineering of plants for research and agriculture purposes (Zupan and Zambryski, 1997).

Crown Gall and *A. tumefaciens*-mediated transformation. *A. tumefaciens* was discovered to be the causative agent of crown gall disease in 1907, and since then it has been widely studied. The tumorous phenotype of plants infected by *A. tumefaciens* results from gene products encoded by a segment of DNA, T-DNA, transferred from the bacterium to the plant cell. Crown gall disease is the production of tumors on the stem of various dicotyledonous plants. The overview of *A. tumefaciens* mediated transformation of a plant cell is illustrated in Figure 1.

The transformation products, the T-DNA and the Vir proteins, are located on a large (200kb) tumor inducing plasmid (pTi). The expression of the *vir* genes in *A. tumefaciens* is induced by exudates from wounded plant cells (Engstrom et al., 1987). One of the most potent signals present in high concentrations in wounded plant cell exudates is a phenolic compound acetosyringone (AS) (Bolton et al., 1986). Acetosyringone is sensed by a two-component system, VirA and VirG. VirA is a membrane bound histidine kinase, which autophosphorylates in the presence of AS and transfers the phosphate to VirG. VirG is a transcriptional activator that binds to the *vir* box, which is located upstream of each *vir* promoter and initiates expression of the *vir* genes.

The Vir proteins form the *vir*-T4SS, which mediate the transport of the T-DNA and effector proteins to the plant cell. The T-DNA is delineated by 25 base pair (bp) border repeats and this region is stably integrated into the plant nuclear genome and subsequently expressed. Specific gene products VirD1, VirD2, and VirC nick at the 25 bp border repeats and VirD2 covalently binds to the 5'end of the right border nick site. A single stranded (ss) copy of the T-DNA region called the T-strand, is displaced from the lolr strand of the T-DNA. VirE2 is a ss nucleic acid binding protein that binds to the T-strand protecting it from nuclease degradation during transport. The binding of VirD2 and VirE2 to the T-strand forms the T-complex. The T-complex and two other virulence proteins, VirE3, and VirF are transported to the host cell. VirF is a bacterial F-box protein

exported into the host cell (Schrammeijer et al., 2001) that helps uncoat the T-DNA from VirE2 and VIP1 proteins; VIP1 is host cell protein that facilitates the transport of VirE2 into the nucleus (Tzfira et al., 2001). VirE3 is transported to the nucleus and interacts with transcription factors to induce genes needed for tumor development (Garcia-Rodriguez et al., 2006).

Once transported into the host cell, nuclear localization signals on VirD2 and VirE2 target the T-complex to the nucleus of the cell where the T-strand becomes stably integrated into plant chromosomal DNA. The encoded products on the T-DNA are plant hormones such as auxin and cytokinin, and opines which are novel amino acid-sugar conjugates. Plant hormones cause the uncontrolled stimulation of plant cell division, and opines are specifically catabolized by Agrobacteria as a source of carbon and nitrogen. Strains of *A. tumefaciens* can be differentiated based on the opines they produce. The two strains *A. tumefaciens* mostly studied are the nopaline and octopine strains. In addition, opines stimulate conjugation of the Ti plasmid to other *A. tumefaciens* at the wound site. The capacity to transfer DNA to plant cells led to the development of *A.tumefaciens* as a gene vector. Any DNA cloned between the 25 bp repeats can be transferred into plant cells. This transfer process occurs through the *vir*-T4SS of *A. tumefaciens.*

Components of the *vir*-T4SS in *A. tumefaciens*. In *A. tumefaciens*, the *vir*-T4SS assembles a membrane-spanning channel, forming a conduit for substrate translocation and is composed of eleven VirB proteins and VirD4 (Fig. 2). All tIlve components are essential for optimal T-DNA transfer.

VirB1 is a member of a large protein family of lytic transglycosylases present in several secretion systems of Gram-negative bacteria (Koraimann, 2003). Deletion of VirB1 is not absolutely essential, but greatly reduces virulence to less than 3% (Berger and Christie, 1994, Bohne, 1998). The N-terminal domain of VirB1 has homology to lytic transglycosylases and its transglycolase activity is predicted to loosen the peptidoglycan layer and facilitate insertion of the *vir*-T4SS (Zahrl et al., 2005). The C-terminal portion, VirB1*, is processed and secreted to the outside of the bacterial cell. VirB1* is required for T-pilus formation (Zupan et al., 2007).

VirB2 is the major T-pilus component of the *vir*-T4SS. VirB2 is processed from a 121 amino acid prepilin to a 74 amino acid product. The N-terminus of VirB2 is secreted to the periplasm via N-terminal signal peptide. Then a peptide bond between the amino and carboxyl terminal residues results in the final unusual cyclic T-pilin subunit (Eisenbrandt et al., 1999). All VirB proteins are needed to export the T-pilin subunits and form the T-pilus (Lai and Kado, 2000, Zupan et al., 2007). The T-pili are very thin filaments up to 5μm in length with a 10nm outer diameter and a 2nm inner lumen diameter (Lai and Kado, 2002). Mutants of *virB6*, *virB9*, and *virB11*, alloId T-DNA transfer when no detectable T-pilus was observed (Jakubowski et al., 2005, Sagulenko et al., 2001). Deletion of *virB2* prevents T-DNA transfer. It cannot be ruled out that short not detectable T-pili may have been present in the *virB6*, *virB9*, and *virB11* mutants, such that T-pili may have partial function.

VirB3 is a short polypeptide of 108 amino acids with one or two predicted transmebrane segments (Cao and Saier, 2001). VirB3 was predicted to be an outer membrane protein with its C-terminus in the periplasm (Shirasu and Kado, 1993), but recent studies indicate it localizes to the inner membrane with its C and N-termini in the cytoplasm (Mossey et al., 2010). VirB3 is a homolog of the pilin-like protein TraL in *E.coli* (Shirasu and Kado, 1993), and is required for T-pilus assembly and T-DNA secretion (Mossey et al., 2010). Stability of VirB3 requires VirB4, VirB7 and VirB8. It has been proposed to play a role as a sensor for T-pilus assembly (Mossey et al., 2010)

VirB4 homologs are extensively distributed among T4SS in Gram-negative and Gram-positive bacteria. VirB4 is a large inner membrane protein with Walker A and B motifs (Middleton et al., 2005). VirB11 and VirD4 also contain a Walker A motifs. VirB4, VirB11, and VirD4 physically interact and mutation to the Walker A motifs abolishes T-strand and substrate transfer (Atmakuri et al., 2004). The C-terminal portion of the VirB4 hexamer (Atmakuri et al., 2004) resides in the periplasm and is modeled to be directly above the VirB11 hexamer (Draper et al., 2006). In addition, VirB4 also interacts with VirB1, VirB8, and VirB10 (Atmakuri et al., 2004, Draper et al., 2006). VirB4 interactions with VirB3 and VirB8 may facilitate T-pilus formation (Kerr et al, 2010).

VirB5 is a minor component of the T-pilus and is essential for the assembly of the T-pilus (Lai and Kado, 2000, Schmidt-Eisenlohr et al.,1999). Homologs of VirB5 are characteristically 220 residues in length and contain an N-terminal signal peptide, which targets them to the periplasm thorugh the general secretory pathway (T2SS). The structure of a VirB5 homolog, TraC from the IncN palsmid pKM101 has been solved and consists of a three-helix bundle and a globular appendage (Yeo et al., 2003). Structure-function analysis indicates that VirB5 is important for T-DNA transfer. VirB5 is localized at the T-pilus tip (Aly and Baron, 2007) and is postulated to interact with its host cell.

VirB6 is a highly hydrophobic protein with multiple transmembrane domains (Cao and Saier, 2001). VirB6 is essential for the assembly of the T4SS and for transfer of T-DNA (Cascales and Christie, 2004, Jakubowski et al., 2004). VirB6 forms a complex with VirB7, VirB9, and VirB10 (Jakubowski et al., 2003). VirB6 from the nopaline strain stabilizes VirB3 and VirB5, VirB7 and VirB7-VirB7 and VirB7-VirB9 heterodimeres (Hapfelmeier et al., 2000), however the octopine VirB6 had no effect on the accumulation of octopine VirB3, VirB5, VirB8 VirB9, and VirB10 (Judd et al., 2005).

VirB7 is a small lipoprotein protein 56 amino acids is length. VirB7 also contains an N-terminal signal sequence that targets it to the periplasm. VirB7 resides primarily in the outer-membrane and has also been detected in the inner-membrane (Fernandez et al., 1996) and as part of the T-pilus (Sagulenko et al., 2001). VirB7 interacts with itself and forms a disulfide-linked complex with VirB9. VirB7-VirB9 heterodimer stabilizes VirB4, VirB8, VirB9, VIrB10, and VirB11 (Fernandez et al., 1996).

VirB8 is an essential component for the assembly and function of the T4SS. VirB8 is a 238 amino acid protein with a short N-terminal domain in the cytoplasm, a transmembrance helix, and a large C-terminal domain in the

periplasm (Terradot et al., 2004). A yeast two-hybrid study suggests that the periplasmic portion of VirB8 interacts with VirB1, VirB4, VirB9, VirB10, and VirB11 (Ward et al., 2002). Biochemical studies demonstrate that VirB8 interacts with itself, VirB9, and VirB10 (Das and Xie, 2000). Affinity tagging studies of *B. suis* VirB8 demonstrate VirB4 and VirB5 interact with VirB8 (Yuan, 2005). Transfer DNA immunoprecipitation (TrIP) assays demonstrated that VirB8 interacts with T-DNA (Cascales and Christie, 2004). Random mutagenesis demonstrates that five essential amino acids lead to the loss of function of VirB8, and these amino acids mapped to the periplamic domain of VirB8 (Kumar and Das, 2001). The crystal structure of the periplasmic domain predicts surface residues likely to be involved in dimer formation and interaction with other components of the *vir*-T4SS (Bailey et al., 2006). The VirB8 region that may enable protein or DNA interactions is a large conserved region of surface expose residues Arg-109, Glu-110, Val-132, Ala-164, Arg-176, Tyr-222, Gln-223, Ser-225, and Asp-227.

VirB9 is a hydrophilic, 294 amino acid protein with an N-terminal signal sequence for transport through the general secretory pathway. VirB9 is composed of three functional domains. The N-terminal (residues 21 to 116) and C-terminal (residues 186 to 294) domains are highly conserved and necessary for pilus assembly and substrate translocation, however the central domain (residues 126 to 186) is not conserved (Jakubowski et al., 2005). The C-terminal domain of VirB9 is surface exposed (Bayliss et al., 2007).

VirB10 is a bitopic protein 378 amino acids in length. VirB10 contains four domains: a small N-terminal domain that resides in the cytoplasm, a transmembrane α-helix region, a proline-rich region, and a C-terminal β-barrel domain (Jakubowski et al., 2009). Mutations in the N-terminal domain disrupt T-pilus biogenesis without affecting T-DNA transfer. The trans-membrane α-helix region anchors VirB10 in the inner membrane. The proline-rich region promotes the multimer-formation of VirB7, VirB9, and VirB10 complex. The C-terminal β-barrel domain is required for substrate transfer.

The crystal structure of the T4SS core complex revealed that TraF, a VirB10 homolog of the pKM101 plasmid, forms the inner wall of the structure. This places VirB10 as an inner and outer membrane protein, and VirB10 is the only protein in Gram-negative bacteria known to insert to both membranes (Chandran et al., 2009). Fourteen copies of VirB9 together with VirB7 and VirB10 form the “core” of the T4SS complex encoded from the conjugative plasmid pKM101 (Chandran et al., 2009). VirB10 also interacts with other Vir proteins such as VirB1, VirB4, VirB8, VirB11, and VirD4 (Das and Xie, 2000, Ward et al., 2002, Llosa et al., 2003).

VirB11 contains 345 amino acids and resides in the inner membrane independent of other Vir proteins (Rashkova et al., 1997). VirB11 is a member of a large family of ATPases present in bacteria and archea (Planet et al., 2001). VirB11 forms hexameric oligomers, which is a common feature of ATPases. As mentioned above VirB4 and VirD4 also form hexameric oligomers. The C-terminus of VirB4 interacts with the N-terminus of VirB11. As the N-terminus of membrane bound VirB11 is oriented towards the periplasm, VirB4 is modeled to

be located in the periplasm on top of VirB11 (Draper et al., 2006). VirB11 ATPase activity is required for substrate transfer and T-pilus biogenesis (Sagulenko et al., 2001).

VirD4 is a 660 amino acid predominantly cytoplasmic protein, called the coupling protein, that facilitates docking of the T-strand with the rest of the T4SS. VirD4 has two inner membrane-spanning domains (residues 13-30 and 68-86) resulting in a short N-terminal region and a major C-terminal region in the cytoplasm. The cytoplasmic domain contains a nucleotide-binding motif (Gly-x-Gly-x-Gly). The periplasmic and the nucleotide binding domains are required for substrate transfer (Kumar and Das, 2002). VirD4 interacts with the T-strand (Cascales and Christie, 2004). VirD4 also interacts with VirB4, VirB11, and VirB10 (Atmakuri et al., 2004).

Biochemical, genetic, and cell biological studies from these proteins have begun to elucidate the assembly of the T4SS. Therefore the components of the T4SS can be placed into subgroups based on their function. VirB1 is likely one of the first components to arrive at the site of T4SS localization, possibly through interaction with inner membrane localized VirB8. VirB1 likely enables the assembly of the T4SS by cleaving the bacterial cell wall. The energetic complex is composed of VirB4, VirB11, and VirD4. These proteins have ATPase homology, and ATP binding motifs, which may energize the assembly of the *vir*-T4SS and substrate translocation. The core complex, VirB6, VirB7, VirB8, VirB9, and VirB10 span from the inner membrane to the periplasmic space. The extracellular T-pilus major component is VirB2, and its associated proteins are VirB5 at its tip and VirB7 on the cell surface, and VirB3 is essential for pilus biogenesis (Mossey et al., 2010). In DNA immunoprecipitation studies, the T-DNA interacts with Vir proteins in the following order VirD4, VirB11, VirB6, VirB8, VirB9, and VirB2 (Atmakuri et al., 2004). This order determines the translocation pathway of the T-strand through the *vir*-T4SS from the inner to outer membranes.

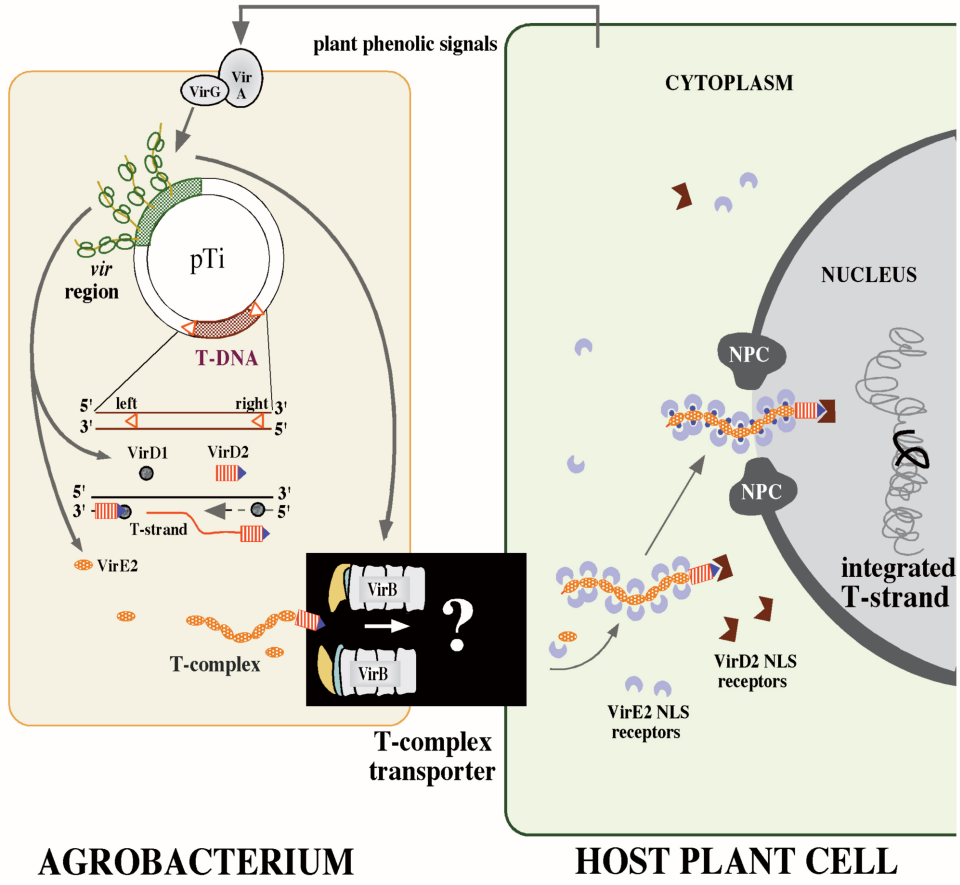

Figure 1. Overview of *Agrobacterium tumefaciens* mediated transformation of a plant cell. See text for details

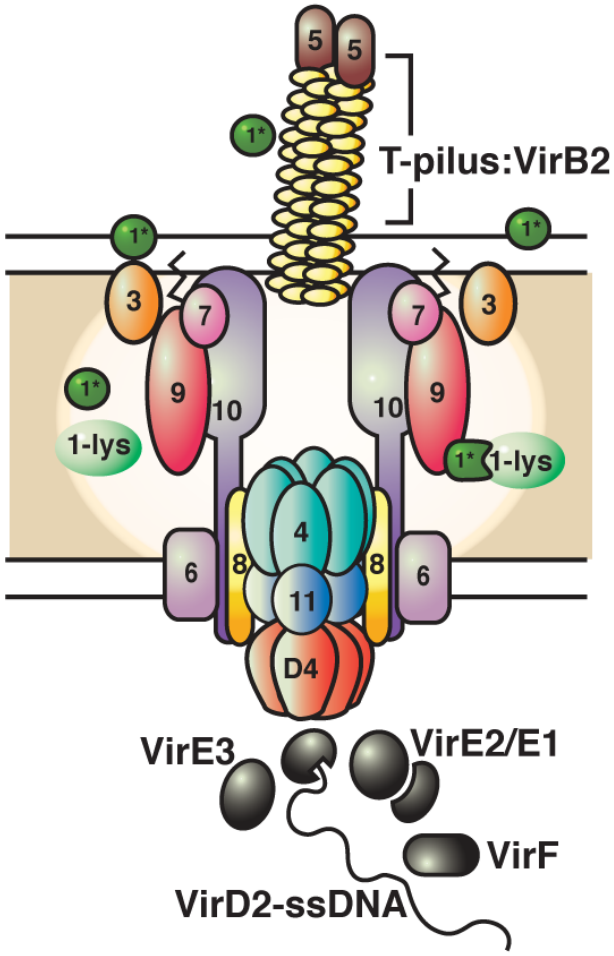

Figure 2. The virulence induced Type IV Secretion System of *Agrobacterium tumefaciens.*

Chapter 2

Agrobacterium type IV secretion system and its substrates form helical arrays around the circumference of *virulence*-induced cells

As published:

AGUILAR, J., ZUPAN, J., CAMERON, T. A. & ZAMBRYSKI, P. C. 2010. Agrobacterium type IV secretion system and its substrates form helical arrays around the circumference of virulence-induced cells. *Proc Natl Acad Sci U S A,* 107**,** 3758-63.

ABSTRACT

The genetic transformation of plant cells by *Agrobacterium tumefaciens* results from the transfer of DNA and proteins via a specific *virulence* (*vir*) induced type IV secretion system (T4SS). To better understand T4SS function I analyzed the localization of its structural components and substrates by deconvolution fluorescence microscopy. GFP fusions to T4SS proteins with cytoplasmic tails, VirB8, VirD4, or cytoplasmic T4SS substrate proteins, VirD2, VirE2, and VirF localize in a helical pattern of fluorescent foci around the perimeter of the bacterial cell. All fusion proteins were expressed at native levels of *vir*-induction. Importantly, most fusion proteins are functional, and do not exhibit dominant negative effects on DNA transfer to plant cells. Further, GFP-VirB8 complements a *virB8* deletion strain. I also detect native VirB8 localization as a helical array of foci by immunofluorescence microscopy. T4SS foci likely use an existing helical scaffold during their assembly. Indeed the bacterial cytoskeletal component MinD co-localizes with GFP-VirB8. Helical arrays of foci are found at all times investigated between 12 and 48 hours post *vir*-induction at 19°C. These data lead to a model with multiple T4SS around the bacterial cell that likely facilitate host cell attachment and DNA transfer. In support, I find multiple T-pili around *vir*-induced bacterial cells.

INTRODUCTION

Agrobacterium tumefaciens is a source of fundamental insights and is intensively utilized due to its ability to transfer any DNA of interest to plant cells (Zupan et al., 2000). The transferred DNA is a single stranded copy of the T-DNA region on its Ti plasmid. A separate region of the Ti plasmid, the *virulence* (*vir*) region, encodes proteins to produce the transferable DNA, and to form a membrane spanning DNA transporter called the type IV secretion system (T4SS. Several Vir proteins, VirD2, VirE2, VirE3, and VirF, are also transported to plants by the *vir*-encoded T4SS (Vergunst et al., 2005).

The transfer of ssDNA to plants via the T4SS is highly evolutionarily conserved, best exemplified by T4SS mediated conjugal ssDNA transfer between bacterial cells. Bacteria have evolved to utilize this ancient mechanism of DNA transfer between bacteria to also transfer DNA or protein toxins into eukaryotic host cells. Important human pathogens such as *Helicobacter pylori, Legionella pneumophila*, *Bordetella pertussis, Brucella suis*, *Bartonella henselae*, and *Ricksettsai prowazekii* transport disease causing factors via T4SSs (Llosa et al., 2009).

T4SS components can be placed into subgroups based on function or location. VirB4, VirB11, and VirD4 have ATPase homology, and ATP binding motifs, which may energize substrate translocation (Atmakuri et al., 2004, Jones et al., 1994, Yeo et al., 2000, Gomis-Ruth et al., 2001) at the inner membrane. VirB3 interacts with VirB4 (Jones et al., 1994). VirB6 is an inner membrane protein, and VirB8 spans the inner membrane placing most of the protein in the periplasm (Kumar et al., 2000, Judd et al., 2005). Recent cryo-electron

microscopy (Fronzes et al., 2009) and crystallography (Chandran et al., 2009) reveal a high resolution structure consisting of 14 copies each of the *Escherichia coli* pKM101 conjugation system VirB7, VirB9, and VirB10 homologs that form a double chambered channel spanning the inner membrane, periplasm, and outer membrane forming the core of the T4SS. VirB2 is the major T4SS pilus component (Lai and Kado, 1998) and the minor component VirB5 (Schmidt-Eisenlohr et al., 1999) localizes at its tip (Aly and Baron, 2007). VirB1 has two domains; the N-terminus has homology to lytic transglycosylases and likely cleaves the peptidoglycan cell wall layer to facilitate assembly of the T4SS (Hoppner et al., 2004, Mushegian et al., 1996, Zahrl et al., 2005); the C-terminal processed portion, VirB1* is secreted to the cell surface (Llosa et al., 2000, Baron et al., 1997) and is required for pilus formation (Zupan et al., 2007).

To understand T4SS function it is critical to determine its localization in the bacterial cell. Several reports suggest that some T4SS proteins localize to one or a few predominantly polar sites (Atmakuri et al., 2003, Atmakuri et al., 2007, Judd, 2005); such localization is proposed to lead to polar substrate transport. However, the results are not entirely consistent as some proteins localize to both poles, the mid-cell, and subpolar regions. Here I use deconvolution microscopy to provide high-resolution images of fluorescent fusions to T4SS components and its secretion substrates. The results reveal that the T4SS localizes to the poles and equally lll as helically arranged foci around the perimeter of the bacterial cell. These data lead to a model where multiple T4SS around the bacterial cell provide multiple sites for interaction with the host cell surface.

RESULTS

I constructed GFP fusions to T4SS components and T4SS substrate proteins. As GFP loses its fluorescence when transported to the periplasm I fused GFP to components that either reside at the cytoplasmic face of the T4SS channel, VirD4, or have predicted cytoplasmic tails, VirB8 and VirB10. Further, I fused GFP to the substrate proteins, VirD2, VirE2 and VirF. As the latter proteins must target to the T4SS for transport, their localization pattern should reflect the localization of the T4SS. The data presented are representative of all cells in a particular optical field, and I analyzed hundreds of cells for each construct; I explicitly state when fewer than 100 % of the cells exhibit a particular pattern.

VirB8 localizes in a helical pattern in vir-induced Agrobacterium

I first assayed the localization pattern of GFP-VirB8. VirB8 has a cytoplasmic N-terminal region of ~40 amino acids, followed by a membrane-spanning domain of ~20 amino acids, and a C-terminal domain of 177 amino acids in the periplasm (Thorstenson and Zambryski, 1994). GFP was fused in frame to the N-terminus of VirB8, sequestering GFP in the cytoplasm, leaving the majority of VirB8 intact in the periplasm allowing for association with other proteins of the T4SS. GFP-VirB8 coding sequences were placed downstream of a *vir*-inducible promoter on the low copy number plasmid pDW029 (Zupan et al., 2007). GFP-VirB8 was transferred into wild type *Agrobacterium* or a deletion of *virB8* (Δ*virB8)*. Following induction of *vir* gene

expression, GFP fusion protein localization was monitored by fluorescence deconvolution microscopy.

Strikingly, widefield images representing groups of bacteria expressing GFP-VirB8 reveals numerous fluorescent foci around the entire perimeter of *vir*-induced cells (Fig. 3D). In contrast, free GFP was evenly distributed throughout the cell (Fig. 3A). GFP-VirB8 appears to zig-zag along the length of the cell with off-set pairs of fluorescent foci (Fig. 3D) suggesting an ordered underlying structure. To better resolve GFP-VirB8, 10-20 optical sections were taken for each bacterial cell and deconvolved to create a three-dimensional (3D) image (Fig. 3E). Figures 3C, 3F, and 3I display individual deconvolved slices from top to bottom through bacterial cells. Movies 1, 2, 3, display rotations of 3D deconvolved stacks. In movies 2 and 3, GFP-VirB8 foci are evident on the perimeter of the cell as expected for a membrane localized T4SS, and there is no GFP-VirB8 in the center of the cell. In contrast free GFP fluorescence is evenly distributed through the entire cell (Fig. 3A-C and movie 1). I generally observe GFP-VirB8 foci with uniform intensity. However, in some images the peripheral fluorescent foci appear stronger when they are closest to the edge of the cell.

The GFP-VirB8 foci appear to be arranged in a helical pattern that winds around the cell. The images of GFP-VirB8 foci are similar to those published for helically arranged bacterial proteins such as MreB (Shih and Rothfield, 2006), MinD (Shih et al., 2003) (see also Fig. 4, below), LytE (Carbadillido-Lopez, 2006), RNAseE (Taghbalout, 2007), SecA (Campo et al., 2004). Many of these bacterial proteins were once thought to reside at single/few mostly polar foci; however, higher resolution microscopy suggests a more complex helical arrangement. Given the numerous constitutive helical array complexes in the bacterial cell, the *vir*-induced T4SS likely associates with such scaffolds rather than itself forming a helical array.

Importantly, an identical helical pattern of fluorescent foci is observed when the GFP-VirB8 construct is expressed in trans to the Ti plasmid in a Δ*virB8* strain (Fig. 3G-I and movie 3). Further, the GFP-VirB8 fusion rescues an avirulent Δ*virB8* strain and promotes strong levels of tumor formation (Fig. 3P). Thus, GFP-VirB8 is functional, and the helical pattern of fluorescent foci must reflect the wild type distribution of the T4SS. Notably expression of GFP-VirB8 in trans to wild type VirB8 does not interfere with tumor formation (Fig. 3O). In all tumor assays presented, except for GFP-VirB8 in Δ*virB8*, GFP fusion proteins are expressed from a plasmid in trans to the Ti plasmid. Thus, I test whether or not the GFP-fusion proteins exhibit dominant negative interference with tumor formation.

Finally, I present images of native VirB8 detected by immunofluorescence and deconvolution microscopy (Fig. 3J-L) performed by a member of the lab, Todd Cameron. Once again, VirB8 clearly forms a helical array of fluorescent foci (Fig. 3J-L and movie 4). Taken together, our data strongly suggest that VirB8, and thus the T4SS of *Agrobacterium*, is localized in a helical arrangement around the perimeter of *vir*-induced cells.

To document that GFP-VirB8 is produced at biologically relevant levels, I assayed for VirB8 and GFP-VirB8. Indeed, GFP-VirB8 is produced at the same level as native VirB8 in wild type (Fig. 3Q, lanes 1-2) and Δ*virB8* (Fig. 3Q, lane 3). GFP-VirB8 is stably expressed as antibodies to GFP detect only the fusion protein and not lower molecular weight proteins (Fig. 6, lane 5).

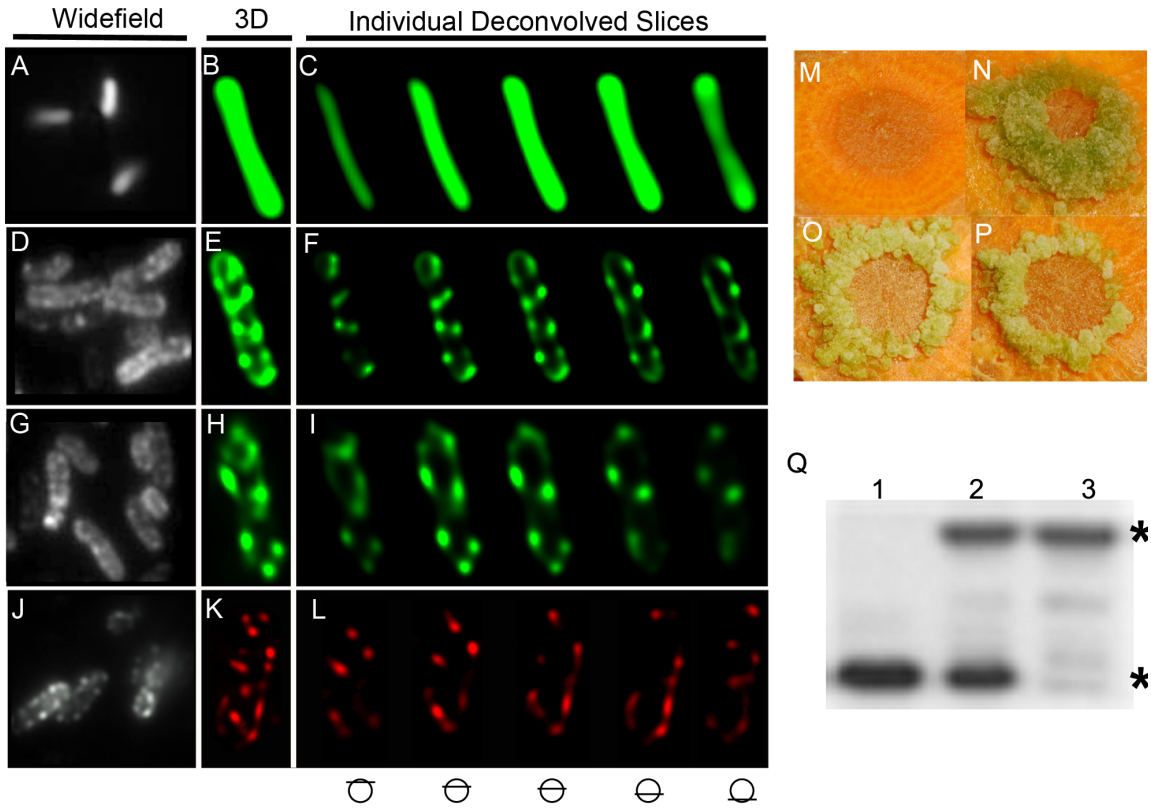

Figure 3. GFP-VirB8 localizes to a helical array of foci in *vir*-induced *Agrobacterium*. (A- C) GFP in wild type *Agrobacterium*. (D-F) GFP-VirB8 in wild type *Agrobacterium*. (G-I) GFP-VirB8 in Δ*virB8*. (J-L) native VirB8 detected with primary rabbit antibodies to VirB8 followed by detection with fluorescent secondary anti-rabbit antibodies. A, D, G, and J are widefield fluorescence images of representative populations of *vir*-induced cells. B, E, H and K are images of a deconvolved 3D stack. C, F, I, and K show 5 sections from top to bottom through the 3D deconvolved images. (M and N) Tumor assays on carrot discs for control (Ti plasmid cured and wild type C58, respectively). (O and P) tumor assays for wild type and Δ*virB8* strains carrying GFP-VirB8, respectively. (Q) documents protein levels of GFP-VirB8 in wild type and Δ*virB8* strains by Western blot using anti-VirB8 antibodies. Lane 1, wild type (C58), lane 2, GFP-VirB8 in C58, lane 3, GFP-VirB8 in Δ*virB8*. * VirB8, 26 kDa, GFP-VirB8, 54 kDa.

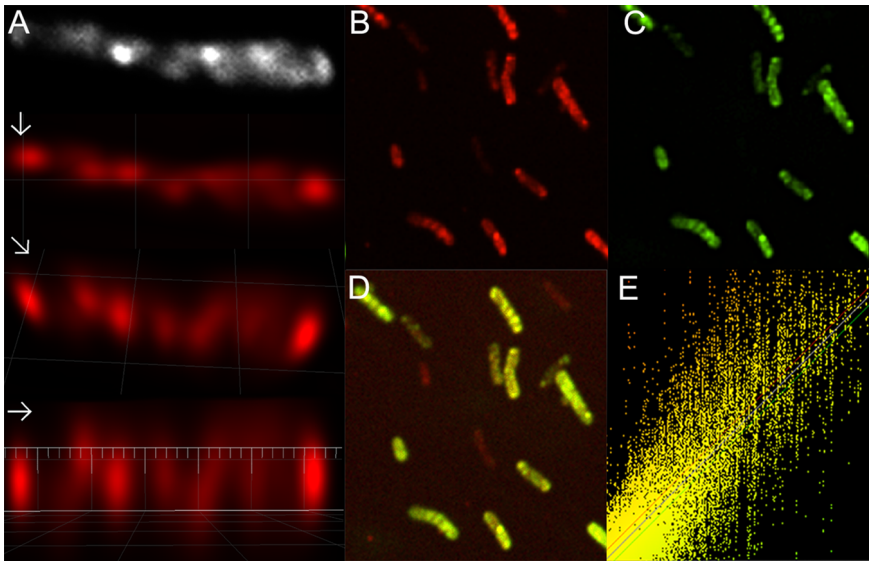

Figure 4. GFP-VirB8 colocalizes with RFP-MinD. (A) shows a deconvolved stack of RFP-MinD, and three different orientations of a deconvolved 3D image. (B-D) GFP-VirB8 and RFP-MinD expressed in the same cells. (B) GFP fluorescence. (C) RFP fluorescence. (D) GFP and RFP colocalization. (E) Scatterplot of green (x-axis) and red (y-axis) pixel intensities used to determine the threshold for colocalization.

Agrobacterium MinD forms helical arrays

I compared the GFP-VirB8 localization pattern with a protein known to form helical arrays. Bacterial cytoskeletal components such as the actin homolog MreB form helical arrays (reviewed in (Shih and Rothfield, 2006)). However, *Agrobacterium* (and other members of the *Rhizobiaceae*) do not contain an MreB homolog (Errington, 2003). Another cytoskeletal protein MinD forms helical arrays (Shih et al., 2003). *Agrobacterium* contains a MinD homolog and fusion to RFP results in helices similar to those observed for VirB8 (Fig. 3D-F).

A member of the lab, John Zupan, tested whether RFP-MinD and GFP-VirB8 arrays co-localize. He cloned RFP-MinD into the plasmid carrying GFP-VirB8. Each fusion is under the control of a copy of the same *vir* promoter, so that RFP and GFP fusion proteins should be expressed at the same level. Indeed, the levels of detection of GFP-VirB8 and RFP-MinD are similar (Fig. 4B-E). Interestingly, the two proteins co-localize, albeit, at the resolution (~100 nm) of light microscopy. The images of RFP-MinD and GFP-VirB8 co-localization were obtained using a spinning disc confocal microscope. These images reveal a more "banded" appearance of MinD and VirB8 than those obtained with the deconvolution microscope; such bands support the helical arrays of foci observed in Figure 3D-L and below.

T4SS substrates VirD2, VirE2, and VirF also localize in a helical pattern in *vir*-induced *Agrobacterium*.

Three T4SS substrate proteins, VirD2, VirE2, and VirF contain C-terminal signal sequences essential for their transport through the T4SS to the plant cell (Vergunst et al., 2005). Thus I made N-terminal GFP fusions to these proteins to preserve their targeting to the T4SS. All three proteins localize in a helical pattern of foci in *vir*-induced cells (Fig. 5A, B, D, E, G, H). GFP-VirF helical arrays are observed in all *vir*-induced cells (Fig. 5D). GFP-VirD2 forms helical arrays in at least 50 % of the cells (Fig. 5A), and GFP-VirE2 forms helical arrays in at least 30 % of the cells (Fig. 5G).

The different degrees of helical pattern formation likely reflect the inherent properties of these substrate proteins, and whether or not GFP interferes with their structure/function. As GFP-VirF does not interfere with tumor formation (Fig. 5F) its 100 % helical localization likely represents wild type VirF function. VirD2 interacts with the T-strand via a conserved tyrosine at position 29 (Balzer et al., 1994), so that an N-terminal GFP fusion may acutely interfere with its localization. However, GFP-VirD2 does not interfere with long-term T4SS function and tumor formation (Fig. 5C). VirE2 is the most abundant Vir protein produced, forms homodimers, heterodimers with VirE1, and complex solenoids in complex with ssDNA (Dym et al., 2008). VirE2 dimers and solenoids are head to tail (N- to C-terminal), so an N-terminal GFP tag likely interferes with mulitmer formation, localization to T4SS helices and tumor formation (Fig. 5I). Or, the abundance of VirE2, coupled with the size of the fusion protein, 95 kDa, may lead to plugging of the T4SS and reduction of tumor formation.

The VirD4 coupling protein forms helical arrays

An important member of the T4SS is the VirD4 coupling protein that escorts the VirD2 bound T-strand to the T4SS (reviewed in (Llosa et al., 2002)). VirD4 association

with VirB11 in the inner membrane is the first step in T-strand transport (Cascales and Christie, 2004). The *E.coli* TrwB homolog of VirD4 forms a hexamer residing in the inner membrane with a C-terminal cytoplasmic tail (Gomis-Ruth et al., 2002). Thus, I made a C-terminal GFP fusion to VirD4. VirD4-GFP also localizes in a helical pattern in *vir*-induced cells (Fig. 5J and K), and allows tumor formation (Fig. 5L). These results support that the C-terminus of VirD4 resides in the cytoplasm and show that fusion to GFP does not interfere with its hexameric structure.

Do GFP fusions to other T4SS components form helical arrays?

As mentioned earlier I also made a GFP fusion to the N-terminus of VirB10 as it has a predicted ~30 amino acid cytoplasmic tail, followed by ~20 amino acid membrane spanning domain, and 327 amino acids in the periplasm (Cascales et al., 2004). However, even though VirB10 has the same general topology as VirB8, it did not form foci (Fig. 6E). Instead, GFP-VirB10 forms a wide band of fluorescence at polar and sub-polar sites around approximately one third of the bacterial cell. This localization pattern is abnormal as GFP-VirB10 is not functional and interferes with tumor formation (Fig. 6F).

Cryo-electron microscopy (Fronzes et al., 2009) and crystallographic studies (Chandran et al., 2009) reveal *E.coli* pKM101 homologs of VirB7, VirB9 and VirB10 are each found in fourteen copies in a complex that spans the periplasm with its ends contacting the inner and outer membrane. Notably, even though VirB7, VirB8, VirB9, and VirB10 were expressed together, VirB8 was not purified along with the core complex (Fronzes et al., 2009). Hence, VirB8 appears not to associate tightly with the VirB7-VirB9-VirB10 core complex.

VirB8 may have more structural flexibility than VirB10, so the addition of GFP to VirB8 does not hinder its function and localization. Remarkably, the independence of VirB8 from the core complex allowed us to detect the formation of GFP-VirB8 helical arrays. The most logical explanation for the lack of helical array formation by GFP-VirB10 is that VirB10 is part of the T4SS multimeric core complex (Fronzes et al., 2009), and its fusion to GFP interferes with its ability to form the core complex.

I also predicted that not all T4SS proteins would fold or function correctly when tagged with GFP. Indeed GFP fusions to VirB4, VirB6, VirB7, VirB9, and VirB11 do not form helical foci, and all exhibit dominant negative effects on tumor formation (Fig. 7). The lack of foci formation for GFP fusions to VirB7 and VirB9 is expected, as these proteins are entirely periplasmic (Fronzes et al., 2009). VirB4 and VirB11 are hexameric ATPases that associate with the inner membrane, and GFP fusion may interfere with their assembly and function. While VirD4 is also a hexameric ATPase, it has a structurally distinct C-terminal cytoplasmic tail (Gomis-Ruth et al., 2002) and GFP fusion did not impair its function or localization. VirB6 is highly hydrophobic with 6 membrane-spanning regions, and GFP may interfere with its folding and function.

The lack of distinct foci formation cannot be explained by degradation of the fusions proteins; while VirB4, VirB6, VirB7, VirB9 and VirB11 fusions display some breakdown products, the expected GFP-fusions represent at least 50 % of their GFP signals (Fig. 6, lanes 2-4 and 6-7, respectively), and while VirD4-GFP displays significant breakdown (Fig. 6, lane 9), it still forms distinct helical arrays of foci (Fig. 5K).

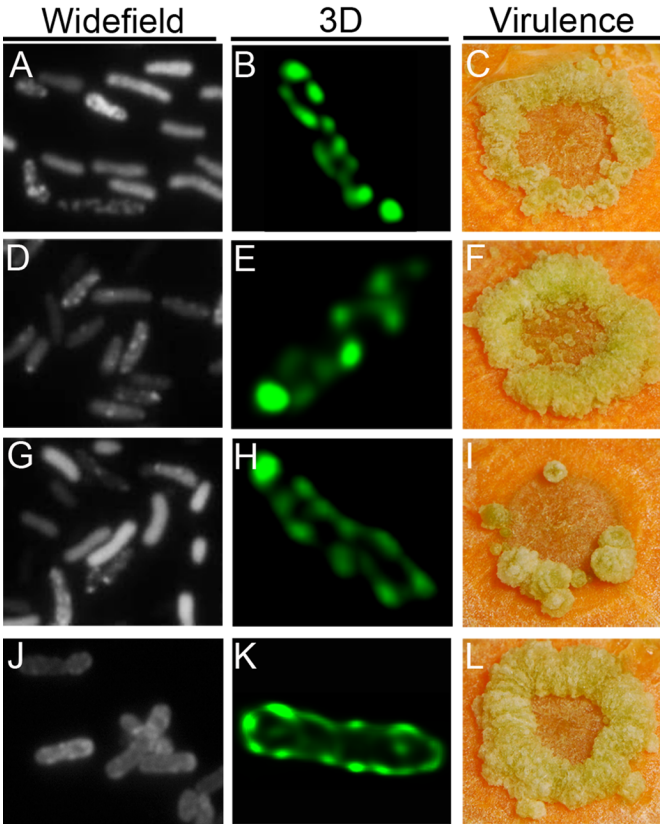

Figure 5. T4SS substrates VirD2, VirF, and VirE2 localize to a helical array of foci in *vir*-induced *Agrobacterium*. (A and B) GFP-VirD2. (D and E) GFP-VirF. (G and H) GFP-VirE2. (J and K) VirD4-GFP. A, D, G, and J are widefield images of representative populations of *vir*-induced cells. B, E, H, and K are 3D deconvolved images. C, F, I, and L show tumor assays on carrot discs for each strain.

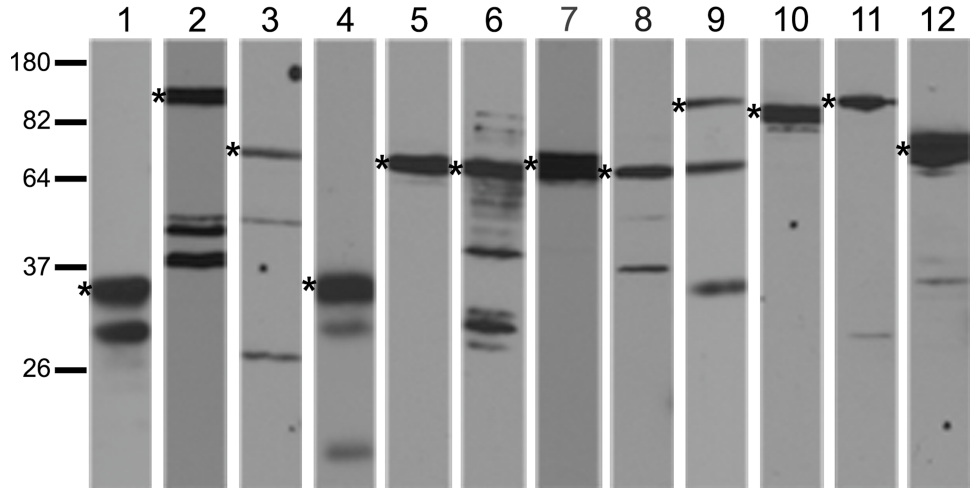

Figure 6. **Expression levels of GFP fusion proteins**. A , Detection of GFP fusion proteins by antibodies to GFP. Lanes 1-12, GFP, VirB4-GFP, VirB6-GFP, VirB7-GFP, GFP-VirB8, VirB9-GFP, GFP-VirB10, VirB11-GFP, VirD4-GFP, GFP-VirD2, GFP-VirE2, GFP-VirF. Proteins from 10^8 cells were loaded into each lane.

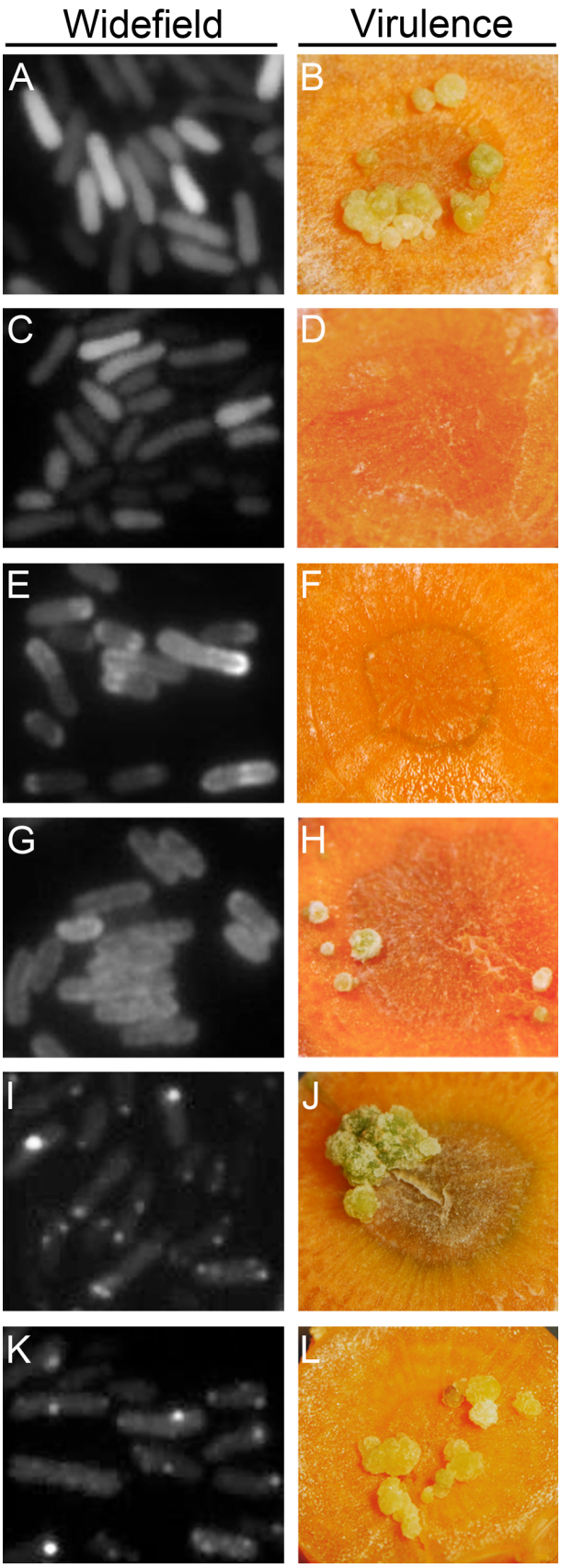

Figure 7. **Localization patterns of GFP fusions to T4SS components, VirB6, VirB7, VirB9, VirB10, VirB11, and VirD4.** A-F, Left panels show widefield fluorescence localization patterns. and right panels show tumor-forming ability. (A and B) VirB7-GFP. (C and D) VirB9-GFP. (E and F) GFP-VirB10. (G and H) VirB6-GFP. (I and J) VirB4-GFP. (K and L) VirB11-GFP.

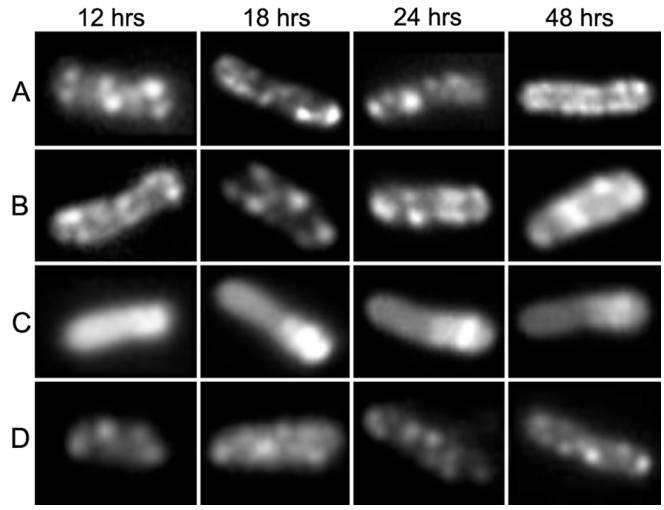

Figure 8. Time course of T4SS and T4SS substrate localization. GFP-VirB8 was localized in wild-type C58 *Agrobacterium* and Δ*virB8*. GFP-VirB10 and GFP-VirF were assayed in wild-type C58 *Agrobacterium*. The cells shown are representative of the localization patterns of fields of cells at 12, 18, 24, and 48 h post *vir* induction. All images are widefield fluorescence. (A) GFP-VirB8 in C58. (B) GFP-VirB8 in CB1008. (C) GFP-VirB10 in C58. (D) GFP-VirF in C58.

Time course of helical localization of the T4SS

The images above (Figures 3-5) were taken following 48 hours of *vir*-induction at 19°C. To determine if these images are representative of T4SS localization at different times following *vir*-induction I performed a time course of GFP-VirB8, GFP-VirB10, and GFP-VirF localization representing a functional helically localized T4SS component, a non-functional GFP fusion that failed to localize in a helical array, and a functional helically localized T4SS substrate, respectively. I also compared the time course of localization of GFP-VirB8 in wild type C58 versus a Δ*virB8* strain. GFP-VirB8 and GFP-VirF form helical arrays at 12, 18, 24 and 48 hours after *vir* gene induction (Fig. 8A-B, and D). The time course of helical localization of GFP-VirB8 is identical in wild type and Δ*virB8*. I have observed such helical arrays as early as 6 hours post *vir*-induction. GFP-VirB10 does not form distinct foci at any time (Fig. 8C).

T-pili localize around the circumference of *vir*-induced *Agrobacterium*

The T4SS is required for the elaboration of an extracellular T-pilus. Thus, it is expected that the T4SS and the T-pilus co-localize. If there are multiple T4SS around the circumference of *vir*-induced *Agrobacterium*, there should be multiple T-pili on the surface of *vir*-induced *Agrobacterium*. Indeed transmission and scanning electron microscopy reveal multiple T-pili around *vir*-induced *Agrobacterium* (Fig. 9A and B, respectively.). I analyzed hundreds of *vir*-induced cells and always observed multiple T-pili around each cell. In the absence of *vir* induction T-pili are not produced (Zupan et al., 2007). As T-pili are extremely fragile, the T-pili observed likely represent a minimal number. I also observe multiple T-pili attaching to the surface of a plant leaf cell (Fig. 9B). For the latter studies, I utilized the so-called “bald” strain of *Agrobacterium* that lacks flagella (Chesnokova et al., 1997) so that all projections from the bacterial surface are T-pili. The plant leaf cell surface removed of its cell wall was obtained following peeling away of the epidermal cell layer from a *Nicotiana benthamiana* leaf, thus presenting an optimal site for high resolution imaging of *Agrobacterium* attachment. *Agrobacterium* was added to the leaf surface immediately after peeling the epidermal layer.

DISCUSSION

The data reveal that induction of *vir* gene expression in *Agrobacterium* results in the production of multiple T4SS that form a helical array of foci around the periphery of the bacterial cell. The helical pattern was observed by fluorescence deconvolution microscopy of GFP fusions to components of the T4SS (VirB8, VirD4) as Ill as to substrate proteins (VirD2, VirE2, VirF) that are transported to plant cells via the T4SS. The helical arrays arise as early as 6-12 hours and remain until at least 48 hours post *vir*-induction. The T4SS helical arrays resemble helical arrays previously observed for bacterial cytoskeletal proteins such as MreB (Shih and Rothfield, 2006), MinD (Shih et al., 2003) as Ill as LytE (Carbadillido-Lopez et al., 2006), RNAseE (Taghbalout et al., 2007), SecA (Campo et al., 2004). I also show that *Agrobacterium* MinD localizes to

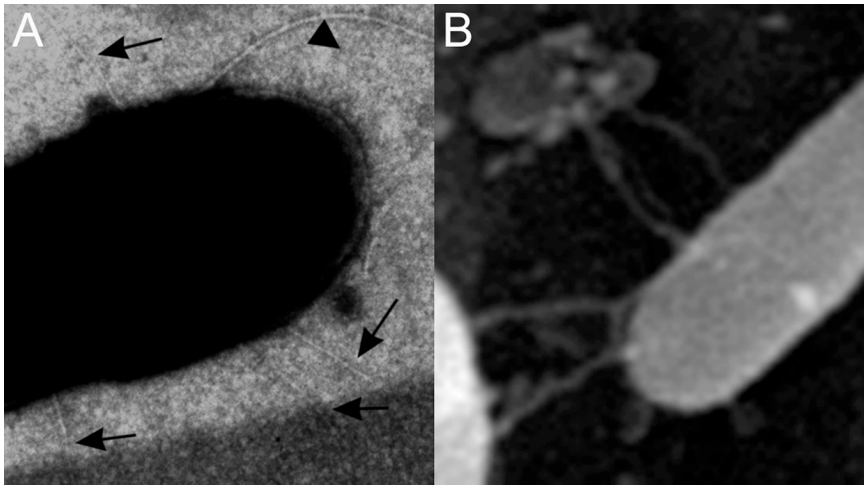

Figure 9. Detection of T-pili in *vir*-induced *Agrobacterium* and during attachment to the plant cell surface. (A) Arrows indicate multiple T-pili around the circumference of *vir*-induced *Agrobacterium*. Top right shows flagellum for comparison (arrowhead). B, Multiple T-pili of the *vir*-induced bald strain of *Agrobacterium* contact the surface of a tobacco leaf cell.

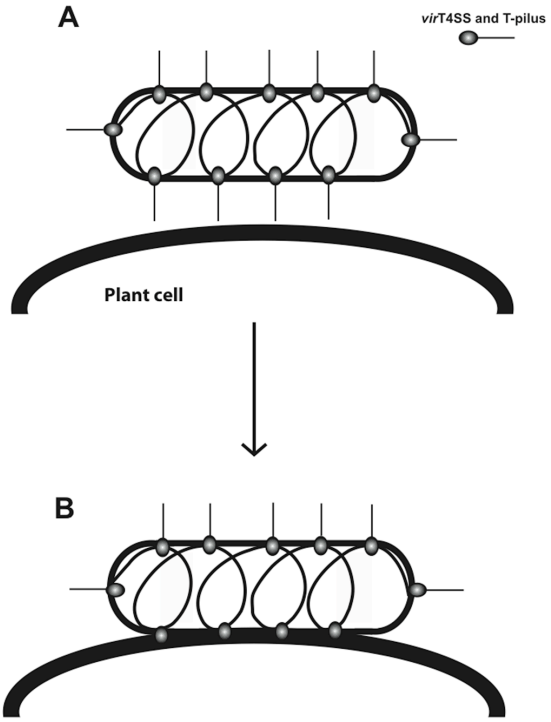

Figure 10. Model for T4SS localization and function during binding to plant cells. *Agrobacterium* with polar and helically localized T4SSs and T-pili make initial contact with a plant cell membrane (thick curved line) (A) and following T-pili retraction multiple T4SS attach to the plant cell surface (B). The T4SS associates with an endogenous helix in the cell.

helical arrays that co-localize with VirB8 in *vir*-induced cells. Thus, the T4SS likely associates with an underlying helical bacterial scaffold.

I suggest two major reasons for previous observations of polar localization of T4SS components and substrates. First, previous studies used standard fluorescence microscopy whereas our results largely were obtained by deconvolution microscopy. The ability to take at least 10 optical sections through a single bacterial cell by deconvolution microscopy allows the cell to be in continuous focus, versus a single image with a limited depth of field. Second, over-expression of bacterial fusions to GFP likely leads to non-specific sequestration to the bacterial poles as inclusion body aggregates (Bardy and Maddock, 2007). GFP-fusions were generated to all open reading frames of *E. coli* and images of cells harboring these plasmids are reported at http://sal.cs.purdue.edu:8097/GB7/GFP/gfp_top.jsp. Amazingly, over 10% of the GFP fusions show polar localization due to the formation of inclusion bodies and are unlikely to have biological meaning. Reports of polar localized GFP fusions to VirD4, VirE2, and VirC1 (Atmakuri et al., 2003, Atmakuri et al., 2007) may result from over-expression from IncP plasmids with copy numbers 5 times higher than the Ti plasmid. In contrast, I employed a plasmid present at only one to two copies per cell (like the Ti plasmid) containing a *vir* inducible promoter active at wild type levels of expression (Zupan et al., 2007). Indeed, GFP-VirB8 is produced in equal quantities compared to the endogenous wild type VirB8.

Importantly, previous reports support multiple foci and helical arrays of the T4SS. First, immuno-gold detection revealed VirB8 around the circumference of the bacterial cell in cross section, and at numerous locations along the length of the cell in longitudinal sections (Thorstenson and Zambryski, 1994). Second, studies of native VirB8, VirB9, and VirB10 detected by fluorescent secondary antibodies revealed striking images of several “foci” arranged in a helical pattern (Kumar et al., 2000). In support for the localization of VirB8 independent of the core VirB7-VirB9-VirB10 complex, VirB8 foci formed in the absence of VirB9 and VirB10, but not vice versa (Kumar et al., 2000).

The helical pattern of T4SS localization leads to a model for T4SS localization and function following attachment to plant cells. Figure 10A shows the T4SS plus associated T-pili around the bacterial cell on a scaffold of an endogenous helically arranged protein complex. T-pili likely facilitate interaction with the host plant cell. By analogy with bacterial conjugation where F-pili retract upon recipient cell contact (Clarke et al., 2008 and reviewed in Firth et al., 1996), T-pili may retract to tether *Agrobacterium* to the plant cell surface. This leads to multiple T4SS in close association with the plant cell surface, thereby maximizing the possibility for effective contacts between bacteria and the plant cell surface for subsequent DNA and protein transfer. In support, conjugating bacteria associate along their lengths and produce electron dense tight junctions spanning contacts between donor and recipient cells (Samuels et al., 2000) and our initial data suggests multiple T-pili associate with the plant cell surface supporting our model for longitudinal binding of *Agrobacterium* to plant cells.

Future studies will address the binding of *Agrobacterium* to plant cells and determine the bases for the co-localization between VirB8 and MinD. VirB8 may be the founding member for T4SS assembly (Kumar et al., 2000, Baron et al.,

2002, Ward et al., 2002), and its association with MinD may initiate the assembly of the VirB7-VirB9-VirB10 core complex. Besides MinD, does the T4SS co-localize with other helically arranged replication proteins (reviewed in (Lutkenhaus, 2007))? Finally, components of the T4SS may co-localize with the Sec secretion system found in helical arrays in other bacteria (Shloml, 2006).

EXPERIMENTAL METHODS

Strains and growth conditions. Wild type *Agrobacterium tumefaciens* strain C58 contains the nopaline pTiC58. CB1008 is a non-polar deletion in pTiC58 *virB8* (Aly et al., 2008). The bald strain is flagella minus (Chesnokova et al., 1997). For *vir* induction an overnight culture was diluted to A_{600} of 0.1 in minimal AB medium (pH 5.5) and grown for 5 h at 19°C (Llosa et al., 2000). Cultures were then plated on AB agar medium containing antibiotics and 200 μM acetosyringone at 19°C.

GFP sequences with 5' BspHI and 3' HindIII restriction sites were inserted into pDW029 (Zupan et al., 2007) to create pJZGFP. Oligonucleotide primers introduced an AvrII restriction site for N-terminal GFP fusions and a BspHI restriction site for C-terminal GFP fusions in pJZGFP. All genes were PCR amplified from pTiC58. Constructs were confirmed by sequencing and transformed into *Agrobacterium* C58.

Imaging. A microscope slide was covered with a thin layer of 1% agarose; then 0.6 -1 μl of cells (in 50 mM potassium phosphate buffer pH 5.5 following re-suspension from plates at A_{600} 2.0) were placed on the agarose pad and covered with a coverslip. Bacteria were viewed with Applied Precision Deltavision Spectris DV4 deconvolution microscope. Stacks of 10-20 optical sections were collected every 0.2 μm on the y-axis. Data (200 iterations) were deconvolved using Huygens software (Scientific Volume Imaging, Hilversum,Netherlands). Three-dimensional structures were modeled using Imaris (Bitplane Scientific Software, Zurich, Switzerland). Co-localization of GFP-VirB8 and RFP-MinD was detected using a Leica DMI6000B inverted microscope equipped with a Yokogawa CSU-10 spinning disc confocal attachment (Yokogawa Electric Corp., Tokyo, Japan) and a Photometrics 512SC EM-CCD camera (Photometrics, Tucson, AZ). Image acquisition was via Metamorph software (Molecular Devices, Sunnyvale, CA) and data were analyzed with the Imaris Co-localization module.

For immunofluorescence cells from induction plates were resuspended to A_{600} 2.0 in AB medium, and fixed in 2.7% paraformaldehyde, 0.01% glutaraldehyde for 15 min at RT and 30 min on ice. Cells were collected, washed with PBS, and stored overnight in 50 mM glucose, 20 mM Tris pH 7.5, 10 mM EDTA. After a PBS wash, cells were permeabilized with PBS containing 2 mg/ml lysozyme, 5 mM EDTA for 45 min at RT. Cells were washed 3X with PBS, then incubated with rabbit anti-VirB8 antibodies in PBS containing 0.1% BSA for 1 h at 37ºC. Following two washes with PBS containing 0.05% Tween-20, secondary antibody incubation was performed with AlexaFluor 546 conjugated to goat anti-rabbit IgG (Invitrogen, Carlsbad, CA) in PBS containing 0.1% BSA for 1 h at

37ºC. Cells were washed 3X with PBS containing 0.05% Tween-20, once with PBS, and resuspended in 200 μl PBS. Cells were imaged as described for GFP fluorescence.

Virulence assay. Carrots sterilized with 20% bleach for 30 min were sliced into 6-10 mm sections and the apical surface was placed on water agar (1.5%) medium. Slices were inoculated with 10 μl (10^9 cells) of *Agrobacterium* harvested from a logarithmic phase culture and suspended in 50 mM PBS. Slices were placed at 20°C for 48 h and then transferred to 24°C. Tumors were photographed 3 to 4 weks after inoculation. All tumor assays are representative of at least 3-independent assays.

Acknowledgements
Thank you Steven Ruzin and Denise Schichnes of the Biological Imaging Facility, William Underwood of the Energy Biosciences Institute, and Reena Zalpuri from the Electron Microscopy lab for yout most valuable advice on microscopy and image analysis. Supported by NSF grant MCB-0343566.

Chapter 3

Membrane and core periplasmic components of the virulence induced type IV secretion system of *Agrobacterium tumefaciens* localize to multiple sites around the bacterial perimeter

(As submitted Aguilar et al, 2011)

ABSTRACT
Type IV secretion systems (T4SS) transfer DNA and/or proteins into recipient cells. Here I performed immunofluorescence deconvolution microscopy to localize the assembled T4SS by detection of its native components, VirB1, VirB2, VirB4, VirB5, VirB7, VirB8, VirB9, VirB10, and VirB11 in the nopaline strain of *Agrobacterium tumefaciens*, C58 following induction of *virulence* (*vir*) gene expression. These different proteins represent T4SS components spanning the inner-membrane, periplasm, or outer-membrane. Native VirB2, VirB5, VirB7, and VirB8 were also localized in the *A. tumefaciens* octopine strain A348. Quantitative analyses of the localization of all the above Vir proteins in nopaline and octopine strains revealed multiple foci in single optical sections in over 80% and 70% of the bacterial cells, respectively. GFP-VirB8 expression following *vir* induction was used to monitor bacterial binding to live host plant cells; bacteria bind predominantly along their lengths, with few bacteria binding via their poles or subpoles. These data support a model where multiple *vir*-T4SS around the perimeter of the bacterium maximize effective contact with the host to facilitate efficient transfer of DNA and protein substrates.

Importance: Transfer of DNA and/or proteins to host cells through multiprotein T4SS complexes that span the bacterial cell envelope is critical to bacterial pathogeneses. Early reports suggested T4SS components localized at the cell poles. Now higher resolution deconvolution fluorescence microscopy reveals that all structural components of *A. tumefaciens vir*-T4SS, as lll as its transported protein substrates, localize to multiple foci around the cell perimeter. These results lead to a new model of *A. tumefaciens* attachment to a plant cell where *A. tumefaciens* takes advantage of the multiple *vir*-T4SS along its length to make intimate plant cell contact and thereby effectively transfer DNA and/or proteins through the *vir*-T4SS. The T4SS of *A. tumefaciens* is among the best-studied T4SS, and the majority of its components are highly conserved in different pathogenic bacterial species. Thus, the results presented can be applied to a broad range of pathogens that utilize T4SS.

INTRODUCTION

Type IV secretion systems (T4SS) are multiprotein complexes used by Gram-negative and Gram-positive bacteria for transfer of DNA and/or proteins to other bacteria (Llosa, 2002, Wallden et al., 2010, Fronzes et al., 2009), plants (Zupan et al., 2000), mammalian (Waters, 2001), and yeast cells (Piers et al., 1996, Bundock et al., 1995). There are two major classes of T4SS. The first class comprises T4SS involved in conjugative transfer of plasmid DNA between bacteria (Llosa et al., 2002, Juhas et al., 2008). The second class is involved in pathogenesis by transferring effector proteins into eukaryotic host cells or the extracellular milieu. Human pathogens such as *Helicobacter pylori*, *Legionella pneumophila*, *Bordetella pertussis*, and *Rickettsai prowazekii*, require the T4SS for disease (Llosa et al., 2009).

The canonical model for T4SS is the virulence (*vir*)-induced T4SS of the plant pathogen *Agrobacterium tumefaciens*. *vir*-T4SS delivers both DNA and proteins into plant cells causing crown gall disease. Components of the *vir*-T4SS are encoded by the tumor inducing plasmid (pTi). The *vir*-T4SS transports pTi encoded single stranded DNA (T-strand) and at least four Vir proteins, VirD2, VirE2, VirE3, and VirF, into host cells. Insertion of the T-strand into plant genomic DNA and its subsequent expression leads to the overproduction of T-DNA encoded plant growth hormones resulting in the tumorous phenotype. Crown gall tumors also produce opines, which are unusual amino acid-derived compounds (Dessaux et al., 1993) specifically catabolized by Agrobacteria as a source of carbon and nitrogen, thus providing a selective advantage for their growth in the rhizosphere (Gelvin et al., 1982, Ooms et al., 1982). Strains of *A. tumefaciens* can be differentiated on the basis of the unique opine produced by the tumor, and each type of opine is specifically catabolized by the infecting strain (Montoya et al., 1977). The two *A. tumefaciens* strains most extensively studied induce tumors that produce the opines nopaline or octopine. The *vir*-T4SS components from these two strains are highly conserved (Christie et al., 2005).

The *vir*-T4SS is composed of eleven VirB proteins (VirB1-11) and VirD4. All VirBs and VirD4 are essential for maximal DNA and protein transport. The *vir*-T4SS components can be placed into three major groups. The first group consists of VirB1 and the T-pilus components. The N-terminal portion of VirB1 has homology to lytic transglycolases and cleaves the peptidoglycan (Zahrl et al., 2005) to facilitate the assembly of the *vir*-T4SS in the periplasmic space. The C-terminus of VirB1, VirB1*, is secreted to the cell surface (Llosa et al., 2000, Baron et al., 1997) and is required for T-pilus formation (Zupan et al., 2007). In addition, VirB3 is required for T-pilus assembly (Jones et al., 1994). VirB2 is the major T-pilus structural component, while the minor component, VirB5, is localized at the T-pilus tip (Aly and Baron, 2007). The second group consists of VirB6-VirB10 that span the inner and outer membranes and periplasm, forming the translocation channel (Das and Xie, 2000). Cryo-electron microscopy and crystal structures show that fourteen copies each of VirB7, VirB9, and VirB10 form a 1.05 M Dalton “core complex” that connects the cytosol to the outer surface of the bacterium with a central core diameter of 76 Å (Chandran, 2009, Fronzes et al., 2009). The arrangement of VirB6 and VirB8 with respect to this core is unknown, but both proteins interact with the T-strand (Cascales and Christie, 2004). The third group consists of VirB4, VirB11, and VirD4, which have ATPase homology and ATP-binding motifs (Atmakuri et al., 2004, Gomis-Ruth et al., 2001, Savvides et al., 2003, Yeo et al., 2000), and may energize assembly and/or substrate translocation. VirD4 is also the coupling protein that brings the T-strand and its associated proteins to the *vir*-T4SS (Cascales et al., 2005, Atmakuri et al., 2003, Kumar and Das, 2002).

To understand *vir*-T4SS function it is critical to determine the localization pattern of the assembled *vir*-T4SS. Previously, I used deconvolution fluorescence microscopy to assess the localization of green fluorescent protein (GFP) fusions to structural components and substrates of the *vir*-T4SS. Due to the bulky nature of GFP very few fusion proteins were functional; this makes

sense given that many T4SS proteins are multimeric or membrane spanning and fusion to GFP is expected to interfere with their assembly. Nevertheless, GFP fusions to the cytoplasmic tails of VirD4 and VirB8 were functional and these GFP fusion proteins localized in a helical pattern of multiple foci around the perimeter of the bacterial cell (Aguilar et al., 2010). However, as there are tIlve *vir*-T4SS components, one might argue that there are sub-assemblies with different localization patterns. Thus, it is critical to determine the localization pattern of the T4SS using probes to all *vir*-T4SS components. Here, antibodies to nine native Vir proteins residing in the inner membrane, periplasm and outer membrane in the nopaline strain C58 were used folloId by immunofluorescence microscopy and detected similar patterns of multiple foci supporting our initial findings. In addition, I extended our studies to the octopine strain A348 and the localization of its *vir*-T4SS is identical to that found in the nopaline strain. Fluorescent labeling of the *vir*-T4SS alloId us to examine the orientation of bacteria during binding to plant and yeast cells. Significant numbers of bacteria bind laterally along their lengths to either host cell and the multiple *vir*-T4SS foci continued to be present during this binding. These data support a model where multiple *vir*-T4SS around the bacterium to maximize effective contact with the host to facilitate efficient transfer of DNA and protein substrates.

RESULTS

Nopaline *vir*-T4SS membrane and periplasmic core structural components localize to multiple foci

Here I use immunofluorescence folloId by deconvolution microscopy to detect nine different structural components of the *vir*-T4SS. The use of antibodies allows localization of the native *vir*-T4SS. In our previous work GFP fusions to VirB8 and VirD4, and to *vir*-T4SS substrate proteins VirD2 and VirF localized to multiple foci in a helical pattern around the circumference of virulence induced cells (Aguilar et al., 2010). Importantly these fusion proteins did not interfere with tumor formation, and GFP-VirB8 rescued a *virB8* deletion (Aguilar et al., 2010). In contrast, GFP fusions to VirB4, VirB6, VirB7, VirB9, VirB10, and VirB11 exhibited dominant negative effects on tumor formation and did not form multiple foci suggesting that the GFP fusion interfered with *vir*-T4SS complex assembly and/or function (Aguilar et al., 2010).

Immunofluorescent detection of nopaline strain specific *vir*-T4SS components, VirB1, VirB2, VirB4, VirB5, VirB7, VirB8, VirB9, VirB10, and VirB11, revealed multiple foci (Fig. 11). Ten optical sections were taken for each bacterial cell and then deconvolved to a three-dimensional (3D) image to better resolve the multiple foci (Fig. 11C). The images recapitulate those seen with GFP-VirB8 fusions (Aguilar et al., 2010) and are suggestive of a helical arrangement of foci. The number of foci varies between a minimum of 10 and a maximum of 19 (Fig. 11C).

Next, thousands of individual cells were analyzed to provide a quantitative assessment of the frequency of multiple foci detected by the nine different antibodies to native nopaline *vir*-T4SS components. As it is impossible to perform

deconvolution microscopy of stacked optical images of thousands of cells, I instead counted foci in a single plane of focus. As shown in Fig. 11B I can easily detect multiple foci, and I specifically assessed the frequency of cells exhibiting 3 or more fluorescent foci. Over 80% of the cells had 3 or more fluorescently labeled foci (Table 1). Most of the cells had between 5 and 10 foci and a very small percentage of cells had only 3 or 4 foci. For example, antibodies to VirB8 showed that 90% of the fluorescently labeled cells contained 3 or more foci reinforcing our results seen with GFP-VirB8 in our earlier report (Aguilar et al., 2010). Antibodies to the T-pilus components, VirB2 and VirB5, revealed that 92% of the fluorescently labeled cells contained 3 or more foci. Antibodies to the energetic components, VirB4 and VirB11, showed that 85% and 83% of the fluorescently labeled cells contained 3 or more foci, respectively. Antibodies to the core components, VirB7, VirB9 and VirB10, showed that 85%, 91% and 89% of the fluorescently labeled cells contained 3 or more foci, respectively.

The labeling specificity of each antibody was significantly higher (p-value <0.05) for *vir*-induced cells (+AS) compared to non-induced cells (-AS) (Table 2). The majority of antibodies labeled less than 7% of non-induced cells signifying high specificity of the antibodies (Table 2). Antibodies to VirB1 and to lesser extent antibodies to VirB7 may have non-specific binding (Table 2). Nevertheless, antibodies to VirB1 detected 3 or more foci in 94% of the fluorescently labeled *vir*-induced cells. Antibodies to VirB7 detected cells with 3 or more foci in 85% of the *vir*-induced nopaline strain cells and 72% of the *vir*-induced octopine strain cells.

Localization of *vir*-T4SS structural components in the Octopine strain

The *vir*-T4SS components are highly conserved among *A. tumefaciens* strains. For example, VirB8 shares 90% amino acid identity between nopaline and octopine strains (Christie et al., 2005). VirB8 has a short N-terminal tail followed by a membrane spanning domain, and the bulk of the C-terminal portion of the protein resides in the periplasm (Thorstenson and Zambryski, 1994). This topology allowed GFP fusion to the VirB8 N-terminus without interference with VirB8 function in the nopaline strain. To test localization of VirB8 in the octopine strain, I made a GFP fusion to the N-terminus of octopine VirB8 and monitored its localization using deconvolution microscopy. Indeed, I detect multiple foci localized around the bacterial cell (Fig. 12) resembling the pattern of GFP-VirB8 fluorescence in the nopaline strain (Aguilar et al., 2010).

Antibodies to VirB2, VirB5, VirB7, and VirB8 from the nopaline strain detect *vir*-induced bands of the predicted molecular lights in extracts of the *vir*-induced octopine strain by western blot analysis (Fig. 12D). Antibody against nopaline VirB8 detects octopine VirB8 at similar levels; interestingly this antibody is not efficient in detecting VirB8 in whole cells by immunofluorescence (Table 2). In contrast, while antibodies against nopaline VirB2, VirB5, and VirB7 were less efficient in detecting their octopine homologs on western blots, these antibodies were effective in detecting their respective proteins in whole cells by immunofluorescence microscopy. Such variation is expected due to the innate

Table 1. Cellular localization of VirB proteins

Strain	Antibody	No. of cells labeled	Percent of cells with ≥3 foci in one optical section
Nopaline	VirB1	504	94
	VirB2	600	92
	VirB4	540	85
	VirB5	450	92
	VirB7	778	85
	VirB8	343	90
	VirB9	94	91
	VirB10	1160	89
	VirB11	315	83
Octopine	VirB2	90	80
	VirB5	145	85
	VirB7	159	72
	VirB8	83	88

Table 2. Labeling specificity of VirB antibodies

Strain		% labeled (Total # cells)	
Nopaline	**Antibody**	**Non-*vir*-induced**	***vir*-induced**
	VirB1	46 (570)	66 (761)
	VirB2	4 (1194)	45 (1341)
	VirB4	2 (752)	66 (823)
	VirB5	7 (609)	69 (654)
	VirB7	19 (593)	56 (1397)
	VirB8	4 (2239)	32 (1064)
	VirB9	2 (487)	8 (1170)
	VirB10	2 (2055)	29 (3970)
	VirB11	5 (265)	59 (531)
Octopine	VirB2	1 (1380)	15 (582)
	VirB5	2 (541)	63 (229)
	VirB7	20 (264)	51 (312)
	VirB8	0 (555)	8 (1081)

*p< 0.05 for all antibodies

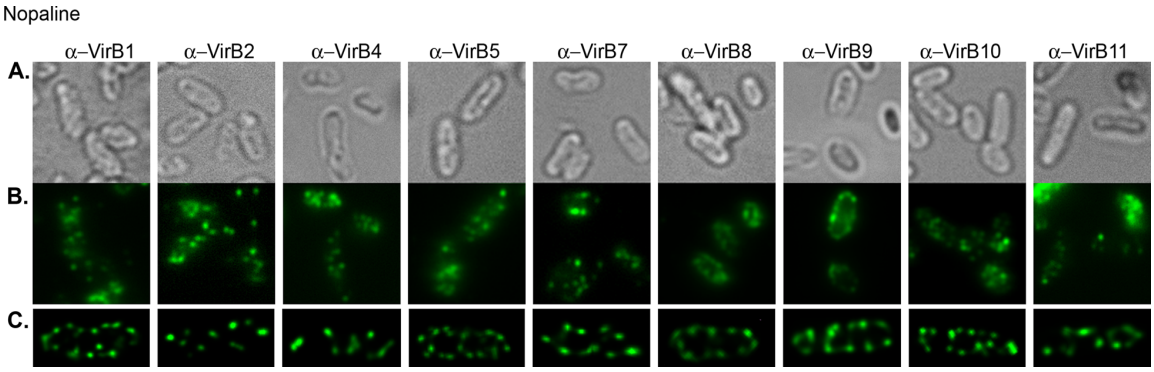

Figure 11. Immunofluorescent detection of VirB proteins in *vir*-induced *A. tumefaciens* nopaline strain (C58). Virulenced induced *A. tumefaciens* C58 were probed with primary antibodies to native VirB proteins (α-VirB1, α-VirB2, α-VirB4, α-VirB5, α-VirB7, α-VirB8, α-VirB9, α-VirB10, α-VirB11) followed by fluorescent secondary antibodies (left to right). A) Bright field images corresponding to fluorescent panels in B. C) Maximum intensity z-projections of deconvolved z-stacks of a representative cell.

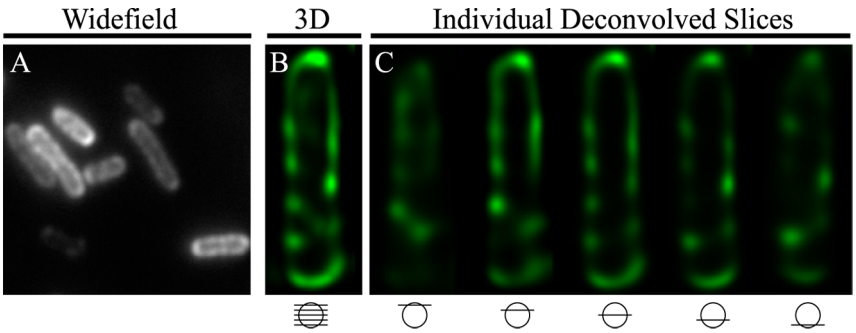

Figure 12. Localization of octopine VirB8 in *vir*-induced *A. tumefaciens* octopine strain (A348). GFP-VirB8 in wild-type *A. tumefaciens* A348. A) Widefield image. B) Maximum intensity z-projections of deconvolved z-stacks of a representative cell. C) Individual deconvolved slices from top to bottom of the cell in panel B.

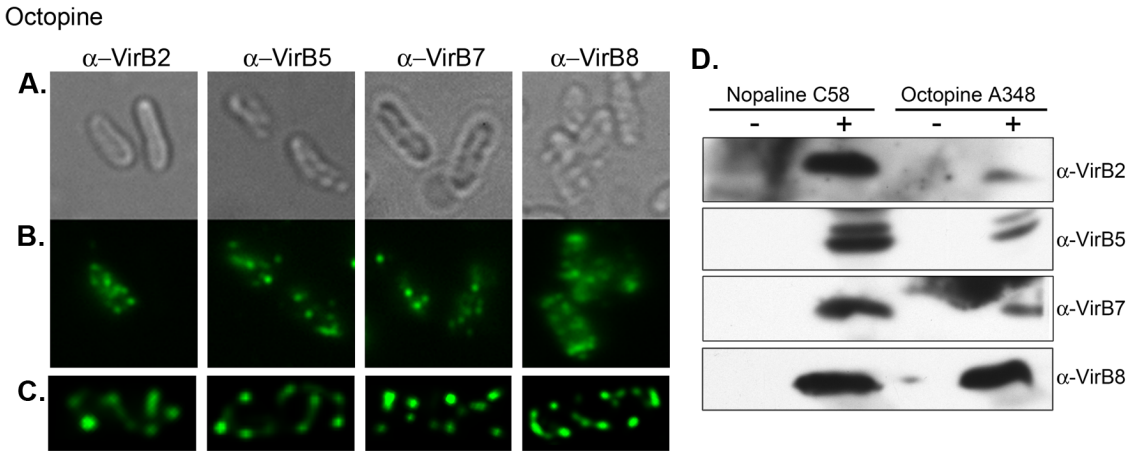

Figure 13. Detection of VirB proteins in *A. tumefaciens* A348. Antibodies from the nopaline strain C58 were used to detect native VirB proteins in the octopine strain A348. A) Bright field images corresponding to fluorescent panels in B. B and C) Immunofluorescence detection with primary antibodies to native A348 VirB proteins (α-VirB2, α-VirB5, α-VirB7, and α-VirB8) followed by fluorescent secondary anitbodies (left to right). C) Maximum intensity z-projections of deconvolved z-stacks of a representative cell. D) *A. tumefaciens* from the nopaline and octopine strains were uninduced (-) or induced with 200μm AS (+) for the expression of *vir*-genes. AS-induced bands of the correct molecular weight were recognized by α-VirB2, α-VirB5, α-VirB7, and α-VirB8.

complexity of epitope conformations. Antibodies against nopaline T-pilus components VirB2 and VirB5 detected multiple foci in 80% and 85% of the *vir*-induced octopine cells (Fig. 13 and Table 1). Similarly antibodies against the nopaline core components VirB7 and VirB8 detected multiple foci in 72% and 88% of *vir*-induced octopine cells (Fig. 13 and Table 1). Nopaline antibodies against VirB2, VirB5, and VirB8 labeled less than 2% of the octopine cells under non-inducing conditions (Table 2). All antibodies used for immunofluorescence microscopy of the octopine strain showed a statistically significant difference between *vir*-induced cells and non-induced cells. In the *vir*-induced cells, over 70% of the labeled cells showed 3 or greater foci (Table 1).

A.tumefaciens binds longitudinally to host cells

Attachment between the host cell and *A. tumefaciens* is necessary for the transfer of the *vir*-T4SS substrates and the T-strand complex. Several reports suggested the *vir*-T4SS localizes to the cell poles (Kumar and Das, 2002, Atmakuri et al., 2003, Judd, 2005, Atmakuri et al., 2007). In addition, an early report of a few *A. tumefaciens* attaching to a single plant cell via their poles lent support for polar attachment (Matthysse, 1987). Even recent reviews continue to suggest polar attachment (Merritt et al., 2007, Tomlinson and Fuqua, 2009) based on these earlier reports. However, our present and previous findings (Aguilar et al., 2010) demonstrate the localization of *vir*-T4SS components, including T-pili, around the circumference of the cell. Multiple *vir*-T4SS suggests that there are multiple points of bacterial attachment to host cells. To test if attachment correlates with the localization of the *vir*-T4SS I used GFP-VirB8 as a marker for the localization of the *vir*-T4SS following incubation of *A. tumefaciens* with three different host cells. *A. tumefaciens* carrying a *vir*-inducible GFP-VirB8 plasmid in trans to pTi were induced for *vir* gene expression with acetosyringone (AS) prior to incubation with host cells. Plant cells are the natural host of *A. tumefaciens* thus I assayed attachment to Bright Yellow-2 (BY2) tobacco culture cells. I made spheroplasts of BY2 cells to mimic the wounded cells that *A. tumefaciens* naturally infects. Bacteria were incubated with plant spheroplasts for 3 hours and binding was monitored by fluorescence deconvolution microscopy. I observed that most bacterial cells bind horizontally along their lengths to the surface of the plant cell, and few bacteria attach in a polar fashion (Fig. 14A). As Agro-infiltration is a common mechanism to introduce constructs for transient or stable expression (Hayward et al., 2011), I also monitored *A. tumefaciens* expressing *vir*-induced GFP-VirB8 following infiltration into *Nicotiana benthamiana* leaf epidermal cells. Once again, I observe *A. tumefaciens* oriented along their lengths in association with plant cells (Fig. 14C).

Additionally, *A. tumefaciens* transforms yeast, *Saccharomyces cerevisiae* (Piers et al., 1996, Bundock et al., 1995), and the smaller size of yeast cells provide better imaging of *A. tumefaciens* attachment (Fig. 14B). I also made yeast spheroplasts and incubated them with *A. tumefaciens* expressing *vir*-induced GFP-VirB8 and observed bacteria bind laterally along their lengths, by their poles, and in a sub-polar manner (at least 1/3 of the bacterial cell is in

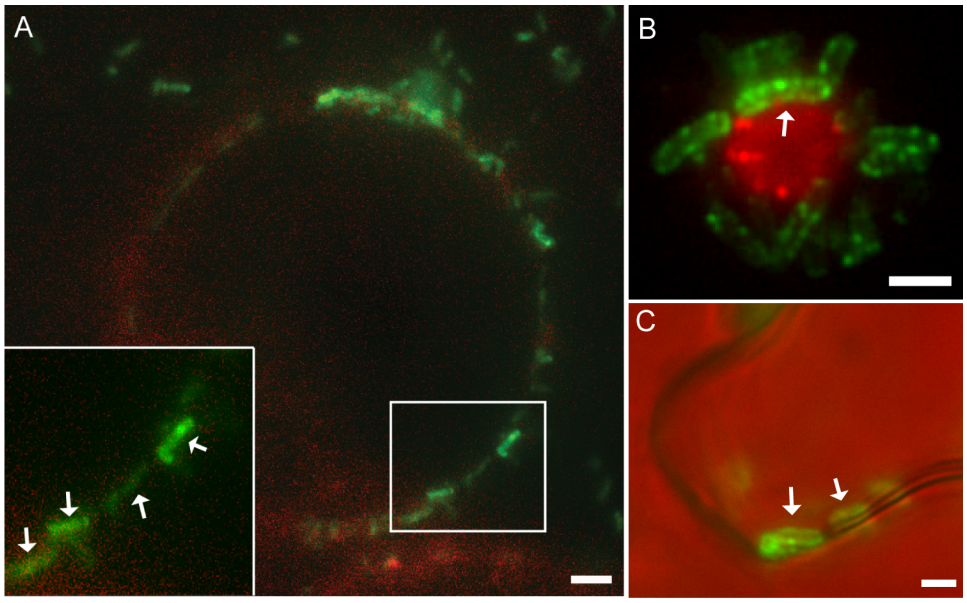

Figure 14. *A. tumefaciens* attachment to host cell(s). *A. tumefaciens* C58 expressing GFP-VirB8 incubated with A) a tobacco BY2 spheroplast, B) yeast spheroplasts or C) infiltrated into an *N. benthamiana* leaf. Arrows indicate bacterial cells that are attached laterally. Scale bars are 2μm.

contact with the yeast). One bacterial cell appears to be making intimate contact, as the bacterial cell is curved to mimic the curvature of the yeast cell (Fig. 14B arrow). Finally, as it is easier to focus on the smaller yeast cells, one can see that the localization of GFP-VirB8 remained in multiple foci following binding (Fig. 14B). Note it is difficult/impossible to focus down on plant cells with attached *A. tumefaciens* as this causes the large and fragile plant cells to burst.

DISCUSSION

Immunofluorescence deconvolution microscopy revealed that the *A. tumefaciens vir*-T4SS is arranged in multiple foci around the circumference of the bacterial cell, supporting our initial findings with GFP fusions to *vir*-T4SS components VirB8, VirD4, and substrates VirD2, VirE2, and VirF (Aguilar et al., 2010). Here, I determined the localization of the *vir*-T4SS by monitoring nine of its components (VirB1, VirB2, VirB4, VirB5, VirB7, VirB8, VirB9, VirB10 and VirB11) in the nopaline strain of *A. tumefaciens*. Over 80% of the fluorescently labeled cells in the nopaline strain showed multiple foci around the bacterial cell. Previously, GFP fusions to the ATPases, VirB4, and VirB11 and core components VirB7, VirB9, and VirB10 interfered with tumor formation; therefore their inability to form multiple GFP foci was not biologically significant (Aguilar et al., 2010). Now, immunofluorescence microscopy using antibodies against these native proteins showed their localization as multiple foci. The spacing of the *vir*-T4SS foci suggests they are helically arranged. Indeed, an independent study to theoretically and experimentally assess the periodicity of the *vir*-T4SS localization pattern supports that *vir*-T4SS are helically arranged (T. Cameron et al, in preparation).

I also extended our localization studies to include VirB1 and T-pili components, VirB2, and VirB5, and all showed similar multi-foci localization patterns in whole cells. I did not detect these proteins in extracellular T-pili. Thus, our antibodies detected both native membrane associated VirB1, VirB2, and VirB5 following the mild fixation used for immunofluorescence, and denatured VirB1, VirB2, or VirB5 on Western blots. Different proteins may change conformation in response to chemical treatments and alter the affinity of antigenic epitopes for the primary antibody. Indeed, following harsh chemical fixation and detection via immunogold electron microscopy, the VirB5 antibody detected denatured VirB5 at T-pili tips, but under these conditions the VirB2 antibody does not detect cell bound T-pili (Aly and Baron, 2007); these authors used VirB2 and VirB5 antibodies from our lab for their studies. Antibodies to VirB1 also labeled a fraction of non-*vir*-induced cells. This nonspecific binding may be due to the recognition of endogenous (non-*vir*) lytic transglycolases or other epitopes with similarity to the C-terminus of the lytic transglycosylase domain of VirB1, the antibody recognition site.

Several authors have observed the localization of *vir*-T4SS components at the bacterial cell poles (Kumar and Das, 2002, Atmakuri et al., 2003, Judd et al., 2005, Atmakuri et al., 2007). These authors used standard wide-field fluorescence microscopy where the low signal to noise ratio may have obscured other foci present on the cell. Standard wide-field fluorescent

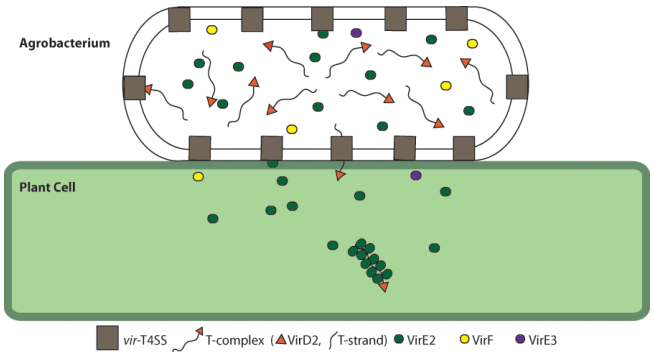

Figure 15. Model for the localization of *vir*-T4SS and lateral attachment of *A. tumefaciens* to a plant cell. It may be advantageous for *A. tumefaciens* to assemble multiple *vir*-T4SS and attach laterally to host cell to facilitate efficient transfer of the 10's of T-complexes and 1,000's of Vir-effector proteins transported through the *vir*-T4SS.

microscopy is limited, as it does not give any information in the Z-dimension. In addition, the earlier reports of polar localization of GFP fusions to VirD4, VirE2, VirC1, and VirB6, may result from over-expression of these proteins from the multicopy IncP plasmid. The over-expression of these proteins would potentially accumulate at the poles in aggregates as seen in *E.coli* (Bardy and Maddock, 2007). For example, in the report of polar VirC1, the bacterial cells were misshapen with large bulges at the poles (Atmakuri et al., 2007). In contrast, our studies with GFP fusions to Vir proteins did not use multicopy plasmids (Aguilar et al., 2010) and herein, and the bacterial cells have the expected rod shape morphology.

Notably, multiple foci along the bacterial cell also have been observed for homologs of the *vir*-T4SS proteins, such as the VirB4 homolog TrhC (Gilmour and Taylor, 2004, Gilmour et al., 2001) and the VirD4 coupling protein homolog TraG (Gunton et al., 2005) from the IncH1 conjugative transfer system of *E. coli*. Immununofluorescence studies showed TrhC and TraG localized at discrete foci around the circumference of the cell membrane.

Here I show that *A. tumefaciens* attaches to plant host cells predominantly by making lateral contacts along their sides with a few bacteria also attaching via their poles or sub-poles. These data suggest that several *vir*-T4SS localized around the bacterial cell may contact the host cell for the transfer of the T-strand and the Vir effector proteins. Earlier observations of *A. tumefaciens* attaching at the poles used intact carrot suspension cells containing cell walls and only monitored few bacteria along the edges of plant cells (Matthysse, 1987). Here I monitored *A. tumefaciens* attachment with plant spheroplasts, as well as following leaf infiltration, which also disrupts plant cell wall connections. Thus, our studies reflect natural circumstances used by *A. tumefaciens* during its transformation of plant cells. *A. tumefaciens* attachment is likely a stepwise dynamic process and the images in Figure 14 represent a snap shot of the attachment progression. Polar and sub-polar attached *A. tumefaciens* may be in transition to become laterally attached or in transition from detaching from the host cell. Nevertheless, our data demonstrates that *A. tumefaciens* attaches laterally to plant cells, in contrast with earlier reports suggesting only polar attachment.

The arrangement of multiple *vir*-T4SS around the bacterial circumference should maximize effective contact between bacteria and host cells. Multiple *vir*-T4SS and lateral attachments may be required to facilitate efficient transfer of T-strands and Vir effector proteins into the host cell (Fig. 15). It is currently estimated that each induced bacterial cell produces 50 T-complexes (Atmakuri et al., 2007). To coat each T-strand would require approximately 30 molecules of VirE2 per kilobase of T-DNA (Zupan et al., 1996, Zambryski, 1992). Therefore, thousands of VirE2 molecules need to be delivered into the host cytoplasm to prevent T-strand degradation. In addition to the numerous VirE2 molecules, VirE3 and VirF proteins also must be translocated through the *vir*-T4SS. Thus, multiple *vir*-T4SS would be advantageous to the bacterial cell to expedite transport of the vast quantities of proteins and T-strands as shown in the model in Figure 15.

MATERIALS AND METHODS

Bacterial Strains and growth conditions

Wild-type *A. tumefaciens* strain C58 contains the nopaline pTiC58 and strain A348 contains octopine pTiA6. For induction of the *vir* system, an overnight culture was diluted to OD_{600} 0.1 in minimal AB medium pH 5.5 and grown for 5 hours at 19°C (Llosa et al., 2000). Cultures were then plated on AB agar plates with 200μM acetosyringone (AS) for 2 days at 19°C.

Western Analysis

Proteins from 10^8 cells were loaded into each lane. After protein separation, gels were transferred to Immobilon-P polyvinylidene difluoride 0.45 μm membranes, and analyzed by standard methods for Western blotting.

Immunofluorescence microscopy

Vir-induced cells were fixed in 3.2% paraformaldehyde and 0.0125% gluteraldehyde for 15 minutes at room temperature. Cells were washed once in GTE (50 mM glucose, 25mM Tris pH 8, 10mM EDTA), pelleted, and resuspended in GTE and stored overnight at 4°C. Cells were washed in GTE and permeabilized by treatment with 2mg/ml of lysozyme and 5mM EDTA for 45 min at room temperature. Primary antibodies were diluted in 1% BSA: anti-VirB1, anti-VirB2, anti-VirB4, anti-VirB5, anti-VirB7 were diluted to (1:50), anti-VirB8 to (1:200), anti-VirB9 to (1:50), anti-VirB10 and anti-VirB11 to (1:100). Antibodies were added individually to each sample and incubated at 37°C for 60 min. The cells were then washed twice with PBS containing 0.05% Tween-20. The secondary antibody, AlexaFluor 488 conjugated to goat anti-rabbit IgG, was added and the samples were incubated at 37°C for 60 min. Cells were washed three times in PBS containing 0.05% Tween-20 and once in PBS. Cells were resuspended in PBS and imaged with an Applied Precision Deltavision Spectris DV4 deconvolution microscope as previously described (Aguilar et al., 2010).

A. tumefaciens interaction with host cells

A. tumefaciens C58 containing GFP-VirB8 in *trans* to pTi was grown in AB minimal media with appropriate antibiotics, and induced with 200μm AS for 48 hours as described above. Bacteria were then scraped off plates, resuspended in AB medium. BY2 tobacco spheroplasts were made by treating the culture cells with Spheroplast Enzyme solution (1% cellulase, 0.01% pectolyase, and 0.4M D-mannitol) at pH 5.5 for 150 minutes. BY2 spheroplasts were collected by centrifugation at 900xg for 5 minutes. BY2 spheroplasts were washed twice with ice cold 0.4M mannitol and resuspended in spheroplast medium (66mM calcium chloride, 7mM sodium acetate, 247mM D-mannitol) pH 5.8. *A. tumefaciens* were incubated with BY2 spheroplasts for 3 hours at 19°C. Unbound *A. tumefaciens* were removed by filtration with a Spectra Mesh Nylon filter (pore size 20μm). *S. cerevisiae* spheroplasts were made by incubating yeast cells with 5mg/ml Zymolase for 15 minutes at 30°C. Yeast spheroplasts were collected by

centrifugation for 5 min at 1,000xg. Yeast spheroplasts were washed and resuspended in 1M sorbitiol with 2mM DTT. *A. tumefaciens* were incubated with yeast spheroplasts for 4 hours at 19°C. Unbound bacterial cells were removed by centrifugation for 5 min at 1,000xg. *A. tumefaciens* was infiltrated into a *N. Bentamiana* leaf by first making a small puncture in the leaf surface with a needle, and then using a needleless syringe for infiltration at the puncture site (Hayward et al., 2011). Yeast and plant cells were imaged with an Applied Precision Deltavision Spectris DV4 deconvolution microscope.

Acknowledgments
Thank you Steve Ruzin and Denise Schichnes of the College of Natural Resources Biological Imaging Facility for advice.
This work was supported by a predoctoral fellowship to JA (NIH Grant F31GM089088) and an NSF grant (MCB-0343566) to PZ.

References

AGUILAR, J., ZUPAN, J., CAMERON, T. A. & ZAMBRYSKI, P. C. 2010. Agrobacterium type IV secretion system and its substrates form helical arrays around the circumference of virulence-induced cells. *Proc Natl Acad Sci U S A,* 107**,** 3758-63.

ALY, K. A. & BARON, C. 2007. The VirB5 protein localizes to the T-pilus tips in Agrobacterium tumefaciens. *Microbiology,* 153**,** 3766-3775.

ALY, K. A., KRALL, L., LOTTSPEICH, F. & BARON, C. 2008. The type IV secretion system component VirB5 binds to the trans-zeatin biosynthetic enzyme Tzs and enables its translocation to the cell surface of Agrobacterium tumefaciens. *J Bacteriol,* 190**,** 1595-604.

ATMAKURI, K., CASCALES, E., BURTON, O. T., BANTA, L. M. & CHRISTIE, P. J. 2007. Agrobacterium ParA/MinD-like VirC1 spatially coordinates early conjugative DNA transfer reactions. *Embo J,* 26**,** 2540-51.

ATMAKURI, K., CASCALES, E. & CHRISTIE, P. J. 2004. Energetic components VirD4, VirB11 and VirB4 mediate early DNA transfer reactions required for bacterial type IV secretion. *Mol Microbiol,* 54**,** 1199-1211.

ATMAKURI, K., DING, Z. & CHRISTIE, P. J. 2003. VirE2, a type IV secretion substrate, interacts with the VirD4 transfer protein at cell poles of Agrobacterium tumefaciens. *Mol Microbiol,* 49**,** 1699-713.

BAILEY, S., WARD, D., MIDDLETON, R., GROSSMANN, J. G. & ZAMBRYSKI, P. C. 2006. Agrobacterium tumefaciens VirB8 structure reveals potential protein-protein interaction sites. *Proc Natl Acad Sci U S A*.

BALZER, D., PANSEGRAU, W. & LANKA, E. 1994. Essential motifs of relaxase (TraI) and TraG proteins involved in conjugative transfer of plasmid RP4. *J Bacteriol,* 176**,** 4285-95.

BARDY, S. L. & MADDOCK, J. R. 2007. Polar explorations Recent insights into the polarity of bacterial proteins. *Curr Opin Microbiol,* 10**,** 617-23.

BARON, C., LLOSA, M., ZHOU, S. & ZAMBRYSKI, P. C. 1997. VirB1, a component of the T-complex transfer machinery of *Agrobacteriumtumefaciens*, is processed to a C-terminal secreted product, VirB1. *J Bacteriol,* 179**,** 1203-10.

BARON, C., O'CALLAGHAN, D. & LANKA, E. 2002. Bacterial secrets of secretion: EuroConference on the biology of type IV secretion processes. *Mol Microbiol,* 43**,** 1359-65.

BAYLISS, R., HARRIS, R., COUTTE, L., MONIER, A., FRONZES, R., CHRISTIE, P. J., DRISCOLL, P. C. & WAKSMAN, G. 2007. NMR structure of a complex between the VirB9/VirB7 interaction domains of the pKM101 type IV secretion system. *Proceedings of the National Academy of Sciences,* 104**,** 1673-1678.

BERGER, B. R. & CHRISTIE, P. J. 1994. Genetic complementation analysis of the *Agrobacteriumtumefaciens*virB operon: *virB2* through *virB11* are essential virulence genes. *J Bacteriol,* 176**,** 3646-60.

BOHNE, J. 1998. The Ti plasmid increases the efficiency of Agrobacterium tumefaciens as a recipient in virB-mediated conjugal transfer of an IncQ plasmid. *Proceedings of the National Academy of Sciences,* 95**,** 7057-7062.

BOLTON, G. W., NESTER, E. W. & GORDON, M. P. 1986. Plant phenolic compounds induce expression of the *Agrobacteriumtumefaciens* loci needed for virulence. *Science,* 232**,** 983-5.
BUNDOCK, P., DEN DULK-RAS, A., BEIJERSBERGEN, A. & HOOYKAAS, P. J. 1995. Trans-kingdom T-DNA transfer from Agrobacterium tumefaciens to Saccharomyces cerevisiae. *EMBO J,* 14**,** 3206-14.
CAMPO, N., TJALSMA, H., BUIST, G., STEPNIAK, D., MEIJER, M., VEENHUIS, M., ISTERMAN, M., MULLER, J.P., BRON, S., KOK, J., KUIPERS, O.P., JONGBLOED, J.D.H. 2004. Subcellular sites for bacterial protein export. *Molecular Microbiology,* 53**,** 1583-1599.
CAO, T. B. & SAIER, M. H., JR. 2001. Conjugal type IV macromolecular transfer systems of Gram-negative bacteria: organismal distribution, structural constraints and evolutionary conclusions. *Microbiology,* 147**,** 3201-14.
CARBADILLIDO-LOPEZ, R., FORMSTONE, A., LI, Y., EHRLICH, S.D., NOIROT, P., ERRINGTON, J. 2006. Actin homology MreBH governs cells morphogenesis by localization of the cell wall hydrolase LytE. *Developmental Cell,* 11**,** 399-409.
CASCALES, E., AND CHRISTIE, PJ. 2004. Agrobacterium VirB10, an ATP sensor for type IV secretion. *Proc Natl Acad Sci U S A,* 101**,** 17228-17233.
CASCALES, E., ATMAKURI, K., LIU, Z., BINNS, A. N. & CHRISTIE, P. J. 2005. Agrobacterium tumefaciens oncogenic suppressors inhibit T-DNA and VirE2 protein substrate binding to the VirD4 coupling protein. *Molecular Microbiology,* 58**,** 565-579.
CASCALES, E. & CHRISTIE, P. J. 2004. Definition of a bacterial type IV secretion pathway for a DNA substrate. *Science,* 304**,** 1170-3.
CHANDRAN, V., FRONZES, R., DUQUERROY, S., CRONIN, N.,NAVAZA, J., WAKSMAN, G. 2009. Structure of the outer membrane complex of a type IV secretion system. *Nature,* 462**,** in press.
CHESNOKOVA, O., COUTINHO, J. B., KHAN, I. H., MIKHAIL, M. S. & KADO, C. I. 1997. Characterization of flagella genes of *Agrobacteriumtumefaciens*, and the effect of a bald strain on virulence. *Mol Microbiol,* 23**,** 579-90.
CHRISTIE, P. J. 2001. Type IV secretion: intercellular transfer of macromolecules by systems ancestrally related to conjugation machines. *Mol Microbiol,* 40**,** 294-305.
CHRISTIE, P. J., ATMAKURI, K., KRISHNAMOORTHY, V., JAKUBOWSKI, S. & CASCALES, E. 2005. Biogenesis, architecture, and function of bacterial type IV secretion systems. *Annu Rev Microbiol,* 59**,** 451-85.
CLARKE, M., MADDERA, L., HARRIS, R.L., AND SILVERMAN, P.M. 2008. F-pili dynamics by live-cell imaging. *Proc Natl Acad Sci U S A,* 105**,** 17978-17981.
DAS, A. & XIE, Y. H. 2000. The Agrobacterium T-DNA transport pore proteins VirB8, VirB9, and VirB10 interact with one another. *J Bacteriol,* 182**,** 758-63.
DESSAUX, Y., PETIT, A. & TEMPE, J. 1993. Chemistry and biochemistry of opines, chemical mediators of parasitism. *Phytochemistry (Oxford),* 34**,** 31-38.
DRAPER, O., MIDDLETON, R., DOUCLEFF, M. & ZAMBRYSKI, P. C. 2006. Topology of the VirB4 C Terminus in the Agrobacterium tumefaciens VirB/D4 Type IV Secretion System. *Journal of Biological Chemistry,* 281**,** 37628-37635.

DYM, O., ALBECK, S., UNGER, T., JACOBOVITCH, J., BRANZBURG, A., MICHAEL, Y., FRENKIEL-KRISPIN, D., WOLF, S. G. & ELBAUM, M. 2008. Crystal structure of the Agrobacterium virulence complex VirE1-VirE2 reveals a flexible protein that can accommodate different partners. *Proc Natl Acad Sci U S A,* 105**,** 11170-5.

EISENBRANDT, R., KALKUM, M., LAI, E. M., LURZ, R., KADO, C. I. & LANKA, E. 1999. Conjugative pili of IncP plasmids, and the Ti plasmid T pilus are composed of cyclic subunits. *J Biol Chem,* 274**,** 22548-55.

ENGSTROM, P., ZAMBRYSKI, P., VAN MONTAGU, M. & STACHEL, S. 1987. Characterization of Agrobacterium tumefaciens virulence proteins induced by the plant factor acetosyringone. *J Mol Biol,* 197**,** 635-45.

ERRINGTON, J. 2003. The bacterial actin cytoskeleton. *ASM News,* 63**,** 608-614.

FERNANDEZ, D., DANG, T. A., SPUDICH, G. M., ZHOU, X. R., BERGER, B. R. & CHRISTIE, P. J. 1996. The Agrobacterium tumefaciens virB7 gene product, a proposed component of the T-complex transport apparatus, is a membrane-associated lipoprotein exposed at the periplasmic surface. *J Bacteriol,* 178**,** 3156-67.

FIRTH, N., IPPEN-IHLER, K. & SKURRAY, R. 1996. Structure and function of the F factor and mechanism of conjugation. *In:* NEIDHARDT, F. C. (ed.) *Escherichia coli and Salmonella: Cellular and Molecular Biology.* Washington, D.C.: American Society for Microbiology.

FRONZES, R., SCHAFER, E., WANG, L., SAIBIL, H. R., ORLOVA, E. V. & WAKSMAN, G. 2009. Structure of a type IV secretion system core complex. *Science,* 323**,** 266-8.

GARCIA-RODRIGUEZ, F. M., SCHRAMMEIJER, B. & HOOYKAAS, P. J. 2006. The Agrobacterium VirE3 effector protein: a potential plant transcriptional activator. *Nucleic Acids Res,* 34**,** 6496-504.

GELVIN, S. B., THOMASHOW, M. F., MCPHERSON, J. C., GORDON, M. P. & NESTER, E. W. 1982. Sizes and map positions of several plasmid-DNA-encoded transcripts in octopine-type crown gall tumors. *Proc Natl Acad Sci U S A,* 79**,** 76-80.

GILMOUR, M. W., LAWLEY, T. D., ROOKER, M. M., NEWNHAM, P. J. & TAYLOR, D. E. 2001. Cellular location and temperature-dependent assembly of IncHI1 plasmid R27-encoded TrhC-associated conjugative transfer protein complexes. *Mol Microbiol,* 42**,** 705-15.

GILMOUR, M. W. & TAYLOR, D. E. 2004. A subassembly of R27-encoded transfer proteins is dependent on TrhC nucleoside triphosphate-binding motifs for function but not formation. *J Bacteriol,* 186**,** 1606-13.

GOMIS-RUTH, F. X., MONCALIAN, G., DE LA CRUZ, F. & COLL, M. 2002. Conjugative plasmid protein TrwB, an integral membrane type IV secretion system coupling protein. Detailed structural features and mapping of the active site cleft. *J Biol Chem,* 277**,** 7556-66.

GOMIS-RUTH, F. X., MONCALIAN, G., PEREZ-LUQUE, R., GONZALEZ, A., CABEZON, E., DE LA CRUZ, F. & COLL, M. 2001. The bacterial conjugation protein TrwB resembles ring helicases and F1-ATPase. *Nature,* 409**,** 637-41.

GUNTON, J. E., GILMOUR, M. W., ALONSO, G. & TAYLOR, D. E. 2005. Subcellular localization and functional domains of the coupling protein, TraG, from IncHI1 plasmid R27. *Microbiology,* 151**,** 3549-61.

HAPFELMEIER, S., DOMKE, N., ZAMBRYSKI, P. C. & BARON, C. 2000. VirB6 is required for stabilization of VirB5 and VirB3 and formation of VirB7 homodimers in Agrobacterium tumefaciens. *J Bacteriol,* 182**,** 4505-11.

HAYWARD, A., PADMANABHAN, M. & DINESH-KUMAR, S. P. 2011. Virus-induced gene silencing in nicotiana benthamiana and other plant species. *Methods Mol Biol,* 678**,** 55-63.

HOPPNER, C., LIU, Z., DOMKE, N., BINNS, A. N. & BARON, C. 2004. VirB1 orthologs from Brucella suis and pKM101 complement defects of the lytic transglycosylase required for efficient type IV secretion from Agrobacterium tumefaciens. *J Bacteriol,* 186**,** 1415-22.

JAKUBOWSKI, S. J., CASCALES, E., KRISHNAMOORTHY, V. & CHRISTIE, P. J. 2005. Agrobacterium tumefaciens VirB9, an Outer-Membrane-Associated Component of a Type IV Secretion System, Regulates Substrate Selection and T-Pilus Biogenesis. *Journal of Bacteriology,* 187**,** 3486-3495.

JAKUBOWSKI, S. J., KERR, J. E., GARZA, I., KRISHNAMOORTHY, V., BAYLISS, R., WAKSMAN, G. & CHRISTIE, P. J. 2009. Agrobacterium VirB10 domain requirements for type IV secretion and T pilus biogenesis. *Mol Microbiol,* 71**,** 779-94.

JAKUBOWSKI, S. J., KRISHNAMOORTHY, V., CASCALES, E. & CHRISTIE, P. J. 2004. Agrobacterium tumefaciens VirB6 domains direct the ordered export of a DNA substrate through a type IV secretion System. *J Mol Biol,* 341**,** 961-77.

JAKUBOWSKI, S. J., KRISHNAMOORTHY, V. & CHRISTIE, P. J. 2003. Agrobacterium tumefaciens VirB6 protein participates in formation of VirB7 and VirB9 complexes required for type IV secretion. *J Bacteriol,* 185**,** 2867-78.

JONES, A. L., SHIRASU, K. & KADO, C. I. 1994. The product of the *virB4* gene of *Agrobacteriumtumefaciens* promotes accumulation of VirB3 protein. *J Bacteriol,* 176**,** 5255-61.

JUDD, P. K. 2005. Spatial location and requirements for the assembly of the Agrobacterium tumefaciens type IV secretion apparatus. *Proceedings of the National Academy of Sciences,* 102**,** 11498-11503.

JUHAS, M., CROOK, D. W. & HOOD, D. W. 2008. Type IV secretion systems: tools of bacterial horizontal gene transfer and virulence. *Cell Microbiol,* 10**,** 2377-86.

KERR, J. E. & CHRISTIE, P. J. 2010. Evidence for VirB4-mediated dislocation of membrane-integrated VirB2 pilin during biogenesis of the Agrobacterium VirB/VirD4 type IV secretion system. *J Bacteriol,* 192**,** 4923-34.

KORAIMANN, G. 2003. Lytic transglycosylases in macromolecular transport systems of Gram-negative bacteria. *Cellular and Molecular Life Sciences (CMLS),* 60**,** 2371-2388.

KUMAR, R. B. & DAS, A. 2001. Functional analysis of the *Agrobacterium tumefaciens* T-DNA transport pore protein VirB8. *J Bacteriol,* 183**,** 3636-41.

KUMAR, R. B. & DAS, A. 2002. Polar location and functional domains of the Agrobacterium tumefaciens DNA transfer protein VirD4. *Mol Microbiol,* 43**,** 1523-32.

KUMAR, R. B., XIE, Y. H. & DAS, A. 2000. Subcellular localization of the *Agrobacterium tumefaciens* T-DNA transport pore proteins: VirB8 is essential for the assembly of the transport pore. *Mol Microbiol,* 36**,** 608-17.

LAI, E. M. & KADO, C. I. 1998. Processed VirB2 is the major subunit of the promiscuous pilus of *Agrobacteriumtumefaciens*. *J Bacteriol,* 180**,** 2711-7.

LAI, E. M. & KADO, C. I. 2000. The T-pilus of Agrobacterium tumefaciens. *Trends Microbiol,* 8**,** 361-9.

LAI, E. M. & KADO, C. I. 2002. The Agrobacterium tumefaciens T pilus composed of cyclic T pilin is highly resilient to extreme environments. *FEMS Microbiol Lett,* 210**,** 111-4.

LLOSA, M., GOMIS-RUTH, F.X., COLL,M., AND DE LA CRUZ, F. 2002. Bacterial conjugation: a two-step mechanism for DNA transport. *Molecular Microbiology,* 45**,** 1-8.

LLOSA, M., ROY, C., DEHIO. C 2009. Bacterial type IV secretion systems in human disease. *Molecular Microbiology,* 73**,** 141-151.

LLOSA, M., ZUNZUNEGUI, S. & DE LA CRUZ, F. 2003. Conjugative coupling proteins interact with cognate and heterologous VirB10-like proteins while exhibiting specificity for cognate relaxosomes. *Proc Natl Acad Sci U S A,* 100**,** 10465-70.

LLOSA, M., ZUPAN, J., BARON, C. & ZAMBRYSKI, P. 2000. The N- and C-terminal portions of the *Agrobacterium* VirB1 protein independently enhance tumorigenesis. *J Bacteriol,* 182**,** 3437-45.

LUTKENHAUS, J. 2007. Assemby Dynamics of the bacterial MinCDE system and spatial regulation of the Z ring. *Annu Rev Biochem,* 76**,** 539-62.

MATTHYSSE, A. G. 1987. Characterization of nonattaching mutants of Agrobacterium tumefaciens. *J Bacteriol,* 169**,** 313-23.

MERRITT, P. M., DANHORN, T. & FUQUA, C. 2007. Motility and chemotaxis in Agrobacterium tumefaciens surface attachment and biofilm formation. *J Bacteriol,* 189**,** 8005-14.

MIDDLETON, R., SJOLANDER, K., FOLEY, J., AND ZAMBRYSKI, P. 2005. Predicted hexameric structure of the VirB4 protein from *Agrobacteriumtumefaciens* suggests a model for type IV secretion. *Proc Natl Acad Sci U S A***,** in press.

MONTOYA, A. L., CHILTON, M. D., GORDON, M. P., SCIAKY, D. & NESTER, E. W. 1977. Octopine and nopaline metabolism in Agrobacterium tumefaciens and crown gall tumor cells: role of plasmid genes. *J Bacteriol,* 129**,** 101-7.

MOSSEY, P., HUDACEK, A. & DAS, A. 2010. Agrobacterium tumefaciens type IV secretion protein VirB3 is an inner membrane protein and requires VirB4, VirB7, and VirB8 for stabilization. *J Bacteriol,* 192**,** 2830-8.

MUSHEGIAN, A. R., FULLNER, K. J., KOONIN, E. V. & NESTER, E. W. 1996. A family of lysozyme-like virulence factors in bacterial pathogens of plants and animals. *Proc Natl Acad Sci U S A,* 93**,** 7321-6.

O'CALLAGHAN, D., CAZEVIEILLE, C., ALLARDET-SERVENT, A., BOSCHIROLI, M. L., BOURG, G., FOULONGNE, V., FRUTOS, P., KULAKOV, Y. & RAMUZ, M. 1999. A homologue of the Agrobacterium tumefaciens VirB and Bordetella pertussis Ptl type IV secretion systems is essential for intracellular survival of Brucella suis. *Mol Microbiol,* 33**,** 1210-20.

OOMS, G., BAKKER, A., MOLENDIJK, L., WULLEMS, G. J., GORDON, M. P., NESTER, E. W. & SCHILPEROORT, R. A. 1982. T-DNA organization in homogeneous and heterogeneous octopine-type crown gall tissues of Nicotiana tabacum. *Cell,* 30**,** 589-97.

PIERS, K. L., HEATH, J. D., LIANG, X., STEPHENS, K. M. & NESTER, E. W. 1996. *Agrobacteriumtumefaciens*-mediated transformation of yeast. *Proc Natl Acad Sci U S A,* 93**,** 1613-8.

PLANET, P. J., KACHLANY, S. C., DESALLE, R. & FIGURSKI, D. H. 2001. Phylogeny of genes for secretion NTPases: identification of the widespread tadA subfamily and development of a diagnostic key for gene classification. *Proc Natl Acad Sci U S A,* 98**,** 2503-8.

RASHKOVA, S., SPUDICH, G. M. & CHRISTIE, P. J. 1997. Characterization of membrane and protein interaction determinants of the *Agrobacteriumtumefaciens* VirB11 ATPase. *J Bacteriol,* 179**,** 583-91.

SAGULENKO, E., SAGULENKO, V., CHEN, J. & CHRISTIE, P. J. 2001. Role of Agrobacterium VirB11 ATPase in T-Pilus Assembly and Substrate Selection. *Journal of Bacteriology,* 183**,** 5813-5825.

SAMUELS, A. L., LANKA, E, AND DAVIES, J. 2000. Conjugative juntions in RP4-mediated mating of Escherichia coli. *J. Bacteriol.,* 182**,** 2709-2715.

SAVVIDES, S. N., YEO, H. J., BECK, M. R., BLAESING, F., LURZ, R., LANKA, E., BUHRDORF, R., FISCHER, W., HAAS, R. & WAKSMAN, G. 2003. VirB11 ATPases are dynamic hexameric assemblies: new insights into bacterial type IV secretion. *EMBO J,* 22**,** 1969-80.

SCHMIDT-EISENLOHR, H., DOMKE, N., ANGERER, C., WANNER, G., ZAMBRYSKI, P. C. & BARON, C. 1999. Vir proteins stabilize VirB5 and mediate its association with the T pilus of Agrobacterium tumefaciens. *J Bacteriol,* 181**,** 7485-92.

SCHRAMMEIJER, B., RISSEEUW, E., PANSEGRAU, W., REGENSBURG-TUINK, T. J., CROSBY, W. L. & HOOYKAAS, P. J. 2001. Interaction of the virulence protein VirF of Agrobacterium tumefaciens with plant homologs of the yeast Skp1 protein. *Curr Biol,* 11**,** 258-62.

SHIH, Y. L. & ROTHFIELD, L. 2006. The bacterial cytoskeleton. *Microbiol Mol Biol Rev,* 70**,** 729-54.

SHIH, Y. L., TRUNG, L., ROTHFIELD, L. 2003. Division site selection in Escherichia coli involves dynamic redistribution of Min proteins within coiled structures that extend between the two cell poles. *Proc Natl Acad Sci U S A,* 100**,** 7865-7870.

SHIRASU, K. & KADO, C. I. 1993. Membrane location of the Ti plasmid VirB proteins involved in the biosynthesis of a pilin-like conjugative structure on *Agrobacteriumtumefaciens*. *FEMS Microbiol Lett,* 111**,** 287-94.

SHLOML, D., YOSHIMOTO, M., HOMMA, M., KAWAGISHI, I. 2006. Helical distribution of the bacterial chemoreceptor via colocalization with the Sec protein translocation machinery. *Molecular Microbiology,* 60**,** 894-906.

SHRIVASTAVA, R. & MILLER, J. F. 2009. Virulence factor secretion and translocation by Bordetella species. *Curr Opin Microbiol,* 12**,** 88-93.

TAGHBALOUT, A., ROTHFIELD, L. 2007. RNaseE and other constituents of the RNA degradosome are components of the bacterial cytoskeleton. *Proc Natl Acad Sci U S A,* 104**,** 1667-1672.
TERRADOT, L., DURNELL, N., LI, M., ORY, J., LABIGNE, A., LEGRAIN, P., COLLAND, F. & WAKSMAN, G. 2004. Biochemical characterization of protein complexes from the Helicobacter pylori protein interaction map: strategies for complex formation and evidence for novel interactions within type IV secretion systems. *Mol Cell Proteomics,* 3**,** 809-19.
THORSTENSON, Y. R. & ZAMBRYSKI, P. C. 1994. The essential virulence protein VirB8 localizes to the inner membrane of *Agrobacteriumtumefaciens*. *J Bacteriol,* 176**,** 1711-7.
TOMLINSON, A. D. & FUQUA, C. 2009. Mechanisms and regulation of polar surface attachment in Agrobacterium tumefaciens. *Curr Opin Microbiol,* 12**,** 708-14.
TSENG, T. T., TYLER, B. M. & SETUBAL, J. C. 2009. Protein secretion systems in bacterial-host associations, and their description in the Gene Ontology. *BMC Microbiol,* 9 Suppl 1**,** S2.
TZFIRA, T., VAIDYA, M. & CITOVSKY, V. 2001. VIP1, an *Arabidopsis* protein that interacts with *Agrobacterium* VirE2, is involved in VirE2 nuclear import and *Agrobacterium* infectivity. *EMBO J,* 20**,** 3596-607.
VERGUNST, A. C., VAN LIER, M. C., DEN DULK-RAS, A., STUVE, T. A., OUIHAND, A. & HOOYKAAS, P. J. 2005. Positive charge is an important feature of the C-terminal transport signal of the VirB/D4-translocated proteins of Agrobacterium. *Proc Natl Acad Sci U S A,* 102**,** 832-7.
WALKER, D. H. & YU, X. J. 2005. Progress in rickettsial genome analysis from pioneering of Rickettsia prowazekii to the recent Rickettsia typhi. *Ann N Y Acad Sci,* 1063**,** 13-25.
WALLDEN, K., RIVERA-CALZADA, A. & WAKSMAN, G. 2010. Type IV secretion systems: versatility and diversity in function. *Cell Microbiol,* 12**,** 1203-12.
WARD, D. V., DRAPER, O., ZUPAN, J. R. & ZAMBRYSKI, P. C. 2002. Peptide linkage mapping of the *Agrobacterium tumefaciens vir*-encoded type IV secretion system reveals protein subassemblies. *Proc Natl Acad Sci U S A,* 99**,** 11493-500.
WATERS, V. L. 2001. Conjugation between bacterial and mammalian cells. *Nat Genet,* 29**,** 375-6.
YEO, H. J., SAVVIDES, S. N., HERR, A. B., LANKA, E. & WAKSMAN, G. 2000. Crystal structure of the hexameric traffic ATPase of the *Helicobacterpylori* type IV secretion system. *Mol Cell,* 6**,** 1461-72.
YEO, H. J., YUAN, Q., BECK, M. R., BARON, C. & WAKSMAN, G. 2003. Structural and functional characterization of the VirB5 protein from the type IV secretion system encoded by the conjugative plasmid pKM101. *Proc Natl Acad Sci U S A,* 100**,** 15947-52.
YUAN, Q. 2005. Identification of the VirB4-VirB8-VirB5-VirB2 Pilus Assembly Sequence of Type IV Secretion Systems. *Journal of Biological Chemistry,* 280**,** 26349-26359.
ZAHRL, D., WAGNER, M., BISCHOF, K., BAYER, M., ZAVECZ, B., BERANEK, A., RUCKENSTUHL, C., ZARFEL, G. E. & KORAIMANN, G. 2005. Peptidoglycan

degradation by specialized lytic transglycosylases associated with type III and type IV secretion systems. *Microbiology,* 151**,** 3455-67.
ZAMBRYSKI, P. C. 1992. Chronicles from the *Agrobacterium*-plant cell DNA transfer story. *Annu Rev Plant Physiol Plant Mol Biol,* 43**,** 465-90.
ZHU, W., BANGA, S., TAN, Y., ZHENG, C., STEPHENSON, R., GATELY, J. & LUO, Z. Q. 2011. Comprehensive Identification of Protein Substrates of the Dot/Icm Type IV Transporter of Legionella pneumophila. *PLoS One,* 6**,** e17638.
ZUPAN, J., HACKWORTH, C. A., AGUILAR, J., WARD, D. & ZAMBRYSKI, P. 2007. VirB1* Promotes T-Pilus Formation in the vir-Type IV Secretion System of Agrobacterium tumefaciens. *Journal of Bacteriology,* 189**,** 6551-6563.
ZUPAN, J., MUTH, T. R., DRAPER, O. & ZAMBRYSKI, P. 2000. The transfer of DNA from *Agrobacterium tumefaciens* into plants: a feast of fundamental insights. *Plant J,* 23**,** 11-28.
ZUPAN, J. & ZAMBRYSKI, P. 1997. The *Agrobacterium* DNA transfer complex. *Crit Rev Plant Sci,* 16**,** 279-95.
ZUPAN, J. R., CITOVSKY, V. & ZAMBRYSKI, P. 1996. *Agrobacterium* VirE2 protein mediates nuclear uptake of single-stranded DNA in plant cells. *Proc Natl Acad Sci U S A,* 93**,** 2392-7.